13

Combined Fluorescence Methods to Determine Synapses in the Light Microscope: Multilabel Confocal Laser Scanning Microscopy

FLORIS G. WOUTERLOOD

FLORIS G. WOUTERLOOD • Department of Anatomy, Vrije Universiteit Medical Center, Rm MF-G-136, P.O. Box 7057, 1007 MB Amsterdam, The Netherlands

Abstract: The dimensions of synapses are at or below the resolution limit of classical light microscopy. Under optimal conditions, one can appreciate processes of pre- and postsynaptic neurons that appose each other. Such appositions may be casual only and as such not functional in terms of synaptic communication. As a consequence, until quite recently, electron microscopy was the only means available to determine whether identified neurons synapse with each other. Technological developments, however, have created a middle ground between the strictly separated realms of light and electron microscopy. In this chapter I present a triple-fluorescence approach aimed at identifying the apposition of a presynaptic and a postsynaptic neuron, and simultaneously pinpointing a highly specific synapse-associated marker. This third marker identifies the presence of an active zone, necessary to distinguish casual appositions from functional synapses. Methods involved are neuroanatomical tracing, immunofluorescence, confocal laser scanning, and postacquisition computer processing followed by three-dimensional reconstruction and inspection. In my contribution, I will review the theory and practice involved in triple-labeling confocal fluorescence imaging. I begin by dealing with the dimensions of synapses and the structures involved, and relate the physical limitations of light microscopy to the problem of resolving synaptic structure. I then review the principles of image formation in fluorescence microscopy, and present the conditions that must be fulfilled in order to do sound multilabel confocal laser scanning: fluorochromes, lasers, channels, channel separation, and procedures to recognize and suppress unwanted phenomena such as crosstalk. In order to fully illustrate the points discussed, an actual triple visualization experiment will be described. Finally, I will emphasize several important aspects of "operator awareness", that is, the mind setting necessary to work with an advanced optoelectronic instrument like a confocal microscope and its sophisticated software. An aware user senses when some part of the complicated chain of processes is not producing what it is supposed to produce. If operator awareness is absent, strange results may be obtained.

Keywords: anterograde tracing, crosstalk, deconvolution, emission, excitation, fluorescence, neuron markers, synapses, three-dimensional reconstruction

I. INTRODUCTION

Synapses are at the very focus of neuronal functioning. While today the term synapse has a descriptive, morphological meaning, physiologists instead of neuroanatomists introduced the term long ago to underscore the concept of a functional juxtaposition of two neurons exchanging electrical nervous activity (Foster and Sherrington, 1897). In those days of the *belle époque*, neuroanatomists lacked instruments with sufficient resolution

to study synapses, and the dispute between supporters of the novel neuron doctrine (Waldeyer, 1891) and those entertaining the earlier reticulum doctrine propagated by Gerlach (1858) lingered on for 50 years. The argument was finally settled in favor of the neuron doctrine after the invention of the electron microscope and the parallel development of appropriate preparative histologic techniques. In the early 1950s, the morphological correlate of Foster and Sherrington's functional synapse was revealed by Palade and Palay (1954, 1955). In the electron microscope, the ingredients of a typical central nervous system (CNS) synapse consist of a presynaptic axon terminal or bouton and a postsynaptic element that may be a dendritic spine, dendritic shaft, cell body, or even an axon hillock or axon terminal (Fig. 13.1A). Such a site where the outer membranes of two neurons are closely together will be referred to in this chapter as *juxtaposition* or *apposition.* It is evident that in an environment with a dense packing like that in the CNS, not all appositions can be synapses. Appositions involved in synapses display highly specialized areas with increased electron density: active zones. After the arrival of an action potential at a presynaptic bouton, synaptic vesicles docked at the active zone in this terminal fuse to the presynaptic membrane and release their neurotransmitter content into the synaptic cleft. The membrane postsynaptic to the active zone hosts postsynaptic receptors. Neurotransmitter molecules initiate, via their specific receptor, a chain of molecular events that finally generates an excitatory or inhibitory postsynaptic action potential. The point further exploited in this chapter is that the molecular machinery of the synapse includes unique proteins located pre- or postsynaptically. Excitatory and inhibitory events at synapses require completely different molecular machineries. As a consequence, if it could be possible to visualize a presynaptic axon terminal and its juxtaposed postsynaptic element, and to immunostain simultaneously some of the unique proteins belonging to either the excitatory or the inhibitory kind of molecular machinery (Fig. 13.1B), it might be possible to identify the presence of a synapse in the light microscope and to determine its neurochemical role at the same time. Translated into methodology terms, we need a triple-labeling experiment. We have successfully applied an antibody against ProSAP2/Shank3 as the "third marker" (Wouterlood *et al.*, 2003). ProSAP2/Shank3 is a postsynaptic scaffolding protein involved in positioning the *N*-methyl-D-aspartate (NMDA) receptor at the postsynaptic density of excitatory synapses (Böckers *et al.*, 1999, 2002). For inhibitory synapses, the protein gephyrin, i.e., a scaffolding protein for the gamma-aminobutyric acid A ($GABA_A$) receptor at the postsynaptic density, has been proposed as "third marker" (Sassoë-Pognetto and Fritschy, 2000).

The identification of synapses and their possible neurochemical role was until recently a scientific activity confined exclusively within the domain of the electron microscope (Sesack *et al.*, this volume); however, electron microscopy requires fairly large investments in terms of resources, personnel, time, laboratory equipment, and instrument. Furthermore, as symbolized in the inset in Fig. 13.1A, the electron microscope is a sampling instrument

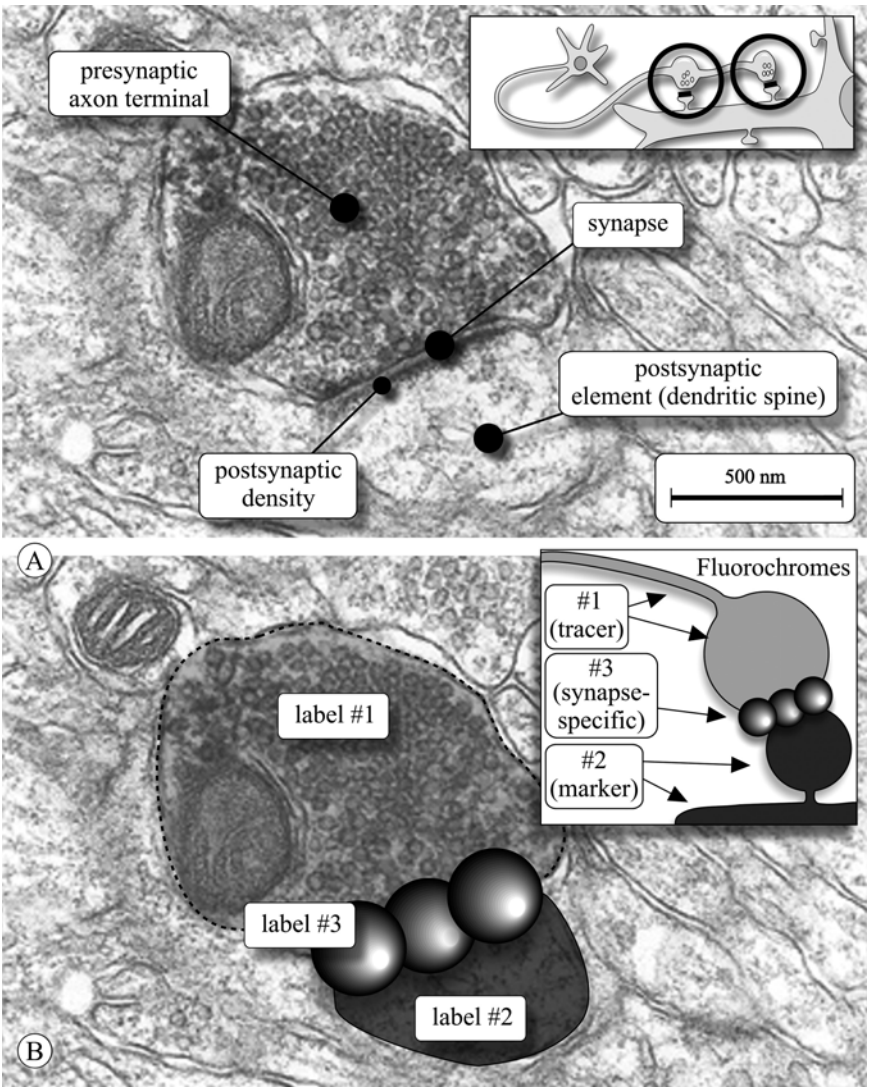

Figure 13.1. (A) Ingredients of a synapse: presynaptic axon terminal, pre- and postsynaptic membrane ("synapse"), postsynaptic element, in this case a dendritic spine. Synapses with marked asymmetry of the membrane specializations are thought to be excitatory. The postsynaptic density contains the molecular scaffolding machinery of the postsynaptic receptors. (B) Concept of a synapse in a light microscopical fluorescence paradigm: labeling of the presynaptic element (marker #1), labeling of the postsynaptic element (label #2, labels #1 and 2 may be neuroanatomical tracers or immunocytochemical markers). Labeling of a synapse-associated protein uniquely present in the postsynaptic density provides label #3. Inset: when fluorochromes are applied, a sandwich of fluorochromes 1, 2, and 3 will show up in the imaging system.

par excellence. Due to its enormous resolution and associated with this the requirement of extremely thin sections, the electron microscope is not the instrument of choice when the purpose of the investigation is to do three-dimensional (3D) reconstruction of large numbers of samples or to see complete neurons including their synapses. The modern confocal laser scanning microscope (CLSM), supplemented with image deconvolution and 3D reconstruction, provides just enough resolution to detect synapses, as will be argued in the following section.

II. THEORETICAL CONSIDERATIONS

A. Can We See Synapses? Practical Implications of Optics Theory

A typical CNS axon terminal is a three-dimensionally organized varicosity with a diameter of 0.5–1.0 μm. The active zone of such a bouton resembles a disk with a diameter of 0.2–0.3 μm and a thickness of approximately 50 nm (Peters *et al.*, 1991). Can we see such small structures in an optical microscope? The resolution of an optical system, or the smallest distance at which two points can be seen as separate points, is given by Ernst Abbe's equation

$$r = 0.61\ \lambda/\mathrm{NA}_{\mathrm{obj}},$$

where the parameter r or lateral resolution distance is measured in the plane perpendicular to the optical axis (Inoué, 1995). Note that there is a wavelength component (λ) and a component related to the quality of the objective lens (NA, numeric aperture). This means that the wavelength of the light used is one of the factors that determine the resolution of the microscope. Based on this formula, with a good 40× dry objective (NA = 0.7), two points seen with blue light ($\lambda = 450$ nm) should be at least 392 nm apart in order to be seen as separate points. With red light ($\lambda = 600$ nm), the minimum distance becomes 522 nm, or 0.5 μm. Note that these are minimum theoretical distances between mathematical points. Such theoretical distances are always smaller than those practically attainable in tissue sections. With a high-quality oil immersion lens (NA = 1.30), the theoretical minimum distances under blue light and red light illumination become 211 and 281 nm, respectively. These numbers illustrate clearly that a synapse is a structure whose size lingers around and below the theoretical resolution limit of a normal light microscope. Because of this constraint, we cannot see under normal conditions with a light microscope whether single molecules in or around the synaptic junction belong to the presynaptic or the postsynaptic compartment. We may see clusters of molecules if such clusters are large enough or when we surround them with sufficient label to create aggregates of staining agent or precipitate in the order of 0.3–0.5 μm. Without doubt, these figures underscore the demand for high-quality objective lenses (high NA) if the aim of the microscope is to look (using bright

or fluorescence light) at very small objects like the synapses between axon terminals and postsynaptic elements.

The above situation is further aggravated for the light microscopist by the fact that light is subject to diffraction. This is the way it is in nature. We have to accept that the projected image from a bright, one-dimensional point onto our eyes, a screen, or a detector is determined by laws of quantum physics and is seen by us and by our instruments as blurred.

Image formation in an optical system is as follows. The wave front of the light, or the photons if light is considered from a quantum physics point of view, distributes in a statistical fashion onto a screen or a detector, with a so-called primary projection maximum surrounded by primary projection minima, secondary projection maxima, secondary projection minima, and so on (Fig. 13.2A). This diffraction pattern is named an Airy distribution, or point spread function (PSF), if one likes to consider light as a stream of photons. The distance between the two primary projection minima in a two-dimensional plot equals the parameter r of Abbe's equation. Since the projection of a stream of photons on a screen is a spot, it is better to refer to the diameter of the disk whose center is the primary projection maximum while the edge is the primary projection minimum. This spot is called the *Airy disk*, and its diameter equals the parameter r of Abbe's equation. It is important to keep in mind that the shape of the diffraction pattern depends on the wavelength of the light involved. Green light ($\lambda =$ 500 nm) has a sharper and narrower distribution curve compared with red light ($\lambda = 600$ nm) (Fig. 13.2B). As a rule of thumb, the higher the energy of the electromagnetic waves, the sharper the peak of the Airy distribution and the better the resolution. Blue light has a shorter wavelength and a higher energy than red light.

Considering two points close to each other, the outcome (r) of Abbe's equation in the previous section should be considered in terms of the distance between the peaks of two partially overlapping Airy distribution curves rather than an absolute distance between two mathematically defined, one-dimensional points. Two distributions of photons can still be distinguished from each other down to a minimum distance. This minimum distance is reached when the primary projection maximum of the first Airy distribution coincides with the first projection minimum of the second Airy distribution (Fig. 13.2C). This minimum distance, which equals the radius of the Airy disk ($1/2$ r of Abbe's equation), is called Rayleigh's criterion (named after Lord Rayleigh who published numerous papers on light theory, e.g., in 1891, on the behavior of light cast through a *pinhole*). The consequence of these physical laws is that a microscopist desperately trying to distinguish two blurred structures from each other by switching to a higher power lens finds that, beyond a certain magnification, this action does not further improve the image.

In classical optical and fluorescence microscopy with its inherent orthoscopic view, the microscopist typically deals with information present in one focal plane. Diffraction is likewise measured, and resolution is expressed

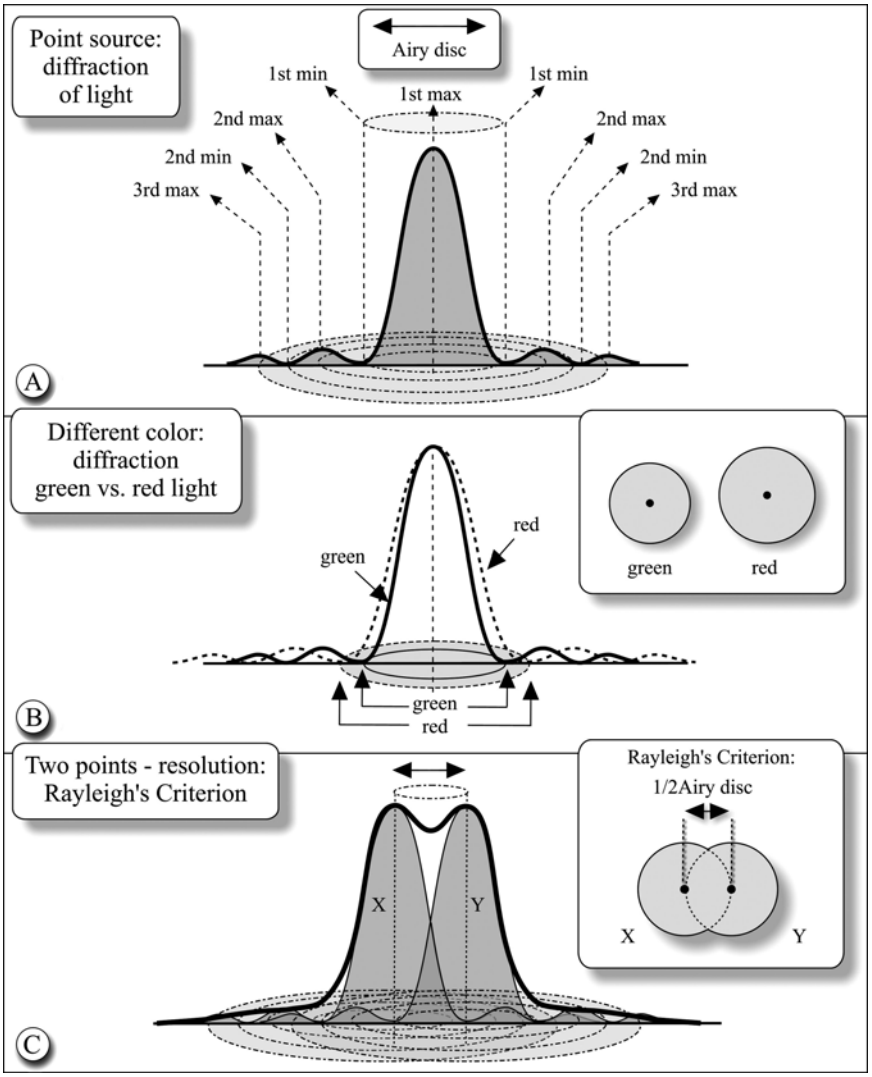

Figure 13.2. Basics of diffraction. (A) Light (photons) projected onto a screen distributes according to a diffraction pattern. The distance between the primary maximum and the first diffraction minimum is called one Airy disk radius. (B) Diffraction is wavelength dependent. The diffraction pattern of light with high energy (short wavelength, e.g., green light) shows a narrower peak than that of light with low energy (long wavelength, e.g., red light). A point light source using green light produces a smaller diffraction spot than that of a point light source using red light. An object "seen" with green light appears therefore smaller than the same object "seen" with red light. (C) Resolution according to Rayleigh's criterion: the smallest distance at which two separate points are still distinguishable as separate entities. The primary maximum of the diffraction pattern of point X coincides with the first diffraction minimum of point Y. This distance equals one Airy radius or half the diameter of the Airy disk. As can be inferred from Panel B, resolution depends on the wavelength of the used light.

in only one optical plane, the *XY* plane. This resolution is also referred to as the "radial resolution." In confocal laser scanning, one typically deals with the distribution of information in a 3D tissue volume. Accordingly, the microscopist has to take into account the axial resolution as well, that is, resolution measured along the optical axis or *Z* axis. This "axial resolution" is lower than that in the radial direction, since the mathematical expression for axial resolution is as follows:

$$r = 2\lambda\acute{\eta}/(\mathrm{NA}_{\mathrm{obj}})^2,$$

where $\acute{\eta}$ is the refractive index of the mounting medium/immersion medium. With blue light (λ = 450 nm) and a high-quality oil immersion lens (NA = 1.30) and using oil immersion ($\acute{\eta} = 1.5$), the theoretical minimum distance between two points in the *Z* direction at which these points are still distinguishable as points is 799 nm. Radial resolution in an optical system is 392 nm (see above), and therefore, it is approximately better than axial resolution by factor 2.

B. Pushing the Envelope: Improvements in Resolution and Image

Two improvements in optics have helped to push the limit of resolution a factor 1.4 down from the theoretically attainable values in a normal optical microscope (Inoué, 1995; Sheppard and Choudhurry, 1977). A third improvement has increased the detail seen by the observer's eyes and has made optical slicing possible. Note that these improvements belong to the category "optical and mathematical tricks" since the underlying fundamental quantum physics cannot be changed.

The first of these improvements is the use of monochromatic light, while the second improvement is postacquisition statistical processing of the signal, called deconvolution. Deconvolution can be considered a sort of reversing the statistics of an Airy distribution. There comes into spotlight the third improvement, which is the CLSM or the sublime instrument implementing these improvements. A laser provides a spot illumination of the object with monochromatic light. The confocal imaging system, whose centerpiece is a pinhole in front of its detectors, blocks haze and other out-of-focus information discomforting to the eye (Fig. 13.3). In-focus images generated by the laser scanning instrument are bitmaps stored on computer hard disk. Postacquisition statistical processing, i.e., deconvolution, "sharpens" the image further in a scientifically valid way.

1. Illumination with Monochromatic Light

The essence of white light is that it is a mixture of light of various wavelengths. As argued above, each wavelength has its own Airy distribution. Illumination of an object via a monochromatic illumination system produces a better image than illumination with white light, since a monochromatic

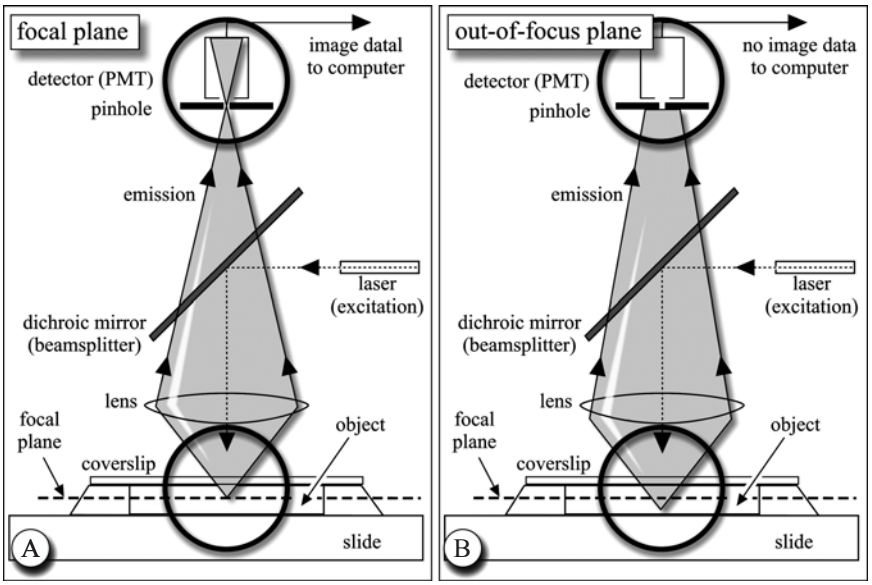

Figure 13.3. The essence of a confocal imaging system is a pinhole in front of the detector. (A) Fluorescence emitted from labeled structures located in the focal plane passes the pinhole and reaches the detector. (B) Emitted light from structures located in all planes other than the focal plane is rejected by the pinhole and does not reach the detector.

illumination system is dealing with only one Airy distribution instead of dealing with many. Furthermore, a lens refracts each wavelength in a slightly different way. The result is the color shift named "chromatic aberration."

Although lenses are usually color corrected to reduce chromatic aberration, the only way to reduce Airy-related blur would be to improve their numeric aperture. However, this parameter is bound by an absolute limit (NA = 1.4). The mixing of Airy distributions associated with different wavelengths combined with a touch of chromatic aberration results in increased blur of the details in the resulting image.

Excitation of a fluorochrome with a monochromatic illumination system avoids the conventional situation in which the object is illuminated with a cocktail of different Airy distributions (at least on the excitation side of the system). It also avoids chromatic aberration. The result is a markedly improved quality of the obtained image. Conventional fluorescence microscopes with their mercury or xenon lamps attempt to achieve via filtering of "excitation lines" from the lamp's light spectrum what a laser does by its very nature. Note that these mercury or xenon excitation lines are always narrow bands of wavelengths and by no means single discrete wavelengths. The fact that in addition to being monochromatic, laser light is also coherent (light waves are in sync) further contributes in a positive way to image formation. To put it simply, the truly monochromatic and coherent light

of a laser produces a result superior to that obtained with a conventional fluorescence microscope. A laser illumination system also produces much better color separation in dual- or multifluorescence applications. The third advantage of a laser is the extremely small beam of high-intensity monochromatic light that can be used to scan a specimen with pulses of light. Note here that the light emitted by the fluorescent specimen is not monochromatic nor coherent. Filtering is necessary to narrow the bandwidth of the emitted light, especially in dual- or multiple-fluorescence applications.

2. Pinhole: Better Resolution at the Cost of Illumination

The most important optical improvement, however, offered by a confocal laser scanning instrument in comparison with a conventional fluorescence microscope is gained by the application of a pinhole in front of the detector. The pinhole is a device that allows only light emitted in a focal plane to pass, whereas emitted light originating from planes above and below the focal plane is rejected (Fig. 13.3; Minsky, 1957; Brakenhoff *et al.*, 1979; Inuoé, 1995). Thus, a confocal instrument possesses an intrinsic mechanism by which out-of-focus light (the major contributor to blur) does not reach the detector. The image looks as if it is sharper (which it is, since all information as well as blur over and under the focal plane is absent).

The diameter of the pinhole has its own effect on resolution, because Rayleigh's criterion also holds for projection apertures. In formula, Rayleigh's criterion applied to a pinhole is expressed as follows:

$$\theta = (1.22\lambda)/D,$$

where θ is the angular separation, λ the wavelength of the used light, and D the diameter of the pinhole. Most important in this respect is the *back-projected pinhole*, that is, the calculated diameter of the real pinhole projected back onto the fluorescence-emitting specimen. It is this back-projected pinhole that really matters and not the real size of the physical pinhole. Most manufacturers of confocal instruments refer in their documentation to this back-projected pinhole when they present data on their instrument's "pinhole." The formula implies that the smaller the pinhole, the better the angular separation, or resolution. Pinholes in general and especially small pinholes reject much light. In fact so much light is blocked by the pinhole (more than 99.99%) that the few photons that manage to pass the pinhole cannot be seen with the naked eye and have to be detected with an expensive and ultrasensitive electronic device: a photomultiplier. Since the emitted light from a fluorescent specimen is a fraction of the light used for excitation, it follows that a section with a fluorescent object needs to be literally flooded with high-intensity light in order to generate enormous number of photons of which only a fraction will ultimately reach the photomultipliers. A drastic measure like saturating a specimen with high-energy excitation light cannot be taken without dire consequences. Bleaching of

the specimen is always a major source of concern. Apart from the application of antifading agents, a solution to bleaching is offered by the two-photon confocal microscope; however, the description of this complex instrument is outside the scope of the present chapter.

3. Intermediate Step: Pixelizing the Image

A photomultiplier is a photon counter and it generates an analogous signal. This signal is digitized and , in conjunction with the scanning movement of the laser beam, used to build up a bitmapped image of the structures of interest. These bitmaps can be further processed with a computer. The projection pattern of an image onto the photomultiplier detector is converted into discrete samples referred to as pixels. A pixel is a square area with a finite size and with a finite intensity level. The light intensity measured in this square area is a gray value, usually a number between 0 and 255 (8-bit intensity sampling) or between 0 and 4095 (12-bit intensity sampling). The size of the pixels compared with the size of the structures to be sampled is important. At this stage of image recording, the sampling rate according to Nyquist comes into the spotlight (Webb and Dorey, 1995). "Nyquist" provides a criterion inasmuch how dense sampling must be in a confocal instrument to satisfy Rayleigh's criterion. The Nyquist sampling rate applied to an Airy distribution implies that sampling must occur at a rate of at least twice the frequency of a distribution curve. In practice, four samples across the Airy disk of a projection diffraction spot originating from a single bright point is the minimum according to Nyquist. The publication by Webb and Dorey (1995) discusses the details of the process of converting a projection image into pixels.

By the application of a pinhole alone, resolution is not pushed beyond the theoretical limit (Inuoé, 1995). It is the contrast of the signal that is being improved and that provides the often-mentioned $\sqrt{2}$ better "resolution" (factor 1.4; Inuoé, 1995). In real-world terms, the theoretical minimum distance at 450 nm illumination (blue light) to distinguish two points in the radial direction is 280 nm, and 570 nm along the Z axis.

4. One Step Beyond Classical Resolution: Deconvolution

A real improvement of the resolution of the optical system is achieved via the combined use of a pinhole (see section "Intermediate Step: Pixelizing the Image") and an additional postacquisition data processing step called deconvolution.

Deconvolution (also called image restoration, deblurring) is, broadly speaking, the postacquisition computational processing of a blurry or noisy image with the purpose to obtain the very best resolution with the highest degree of statistical confidence (Bertero *et al.*, 1990; Holmes *et al.*, 1995; Snyder *et al.*, 1992; van der Voort and Strasters, 1995). As the generation of an Airy distribution of projected light is considered to be a "convolution"

process, the reversal of this process is called "deconvolution." The statistical nature of the generation of an Airy pattern requires that "reversed" statistical calculations be applied in the deconvolution process. Although deconvolution can be performed on single images, this type of processing is in neuroscience mostly applied to *Z* series of confocal images. The reason is that most biological structures extend into three dimensions where, due to the very construction of the instrument, the *X* and *Y* directions have a resolution (radial resolution) different from that along the optical axis (axial resolution, *Z* direction). A *Z* series is a number of images taken in confocal mode. A stepping motor lifts the stage a small, controllable step between each subsequent image. A *Z* series is in fact a series of images each in the narrow focal plane, with the object moving stepwise along the *Z* axis through the focal plane. We will therefore deal with a limited and specialized application of deconvolution, notably the deconvolution of fluorescence images in *Z* series.

5. Three-Dimensional Shape of the PSF in a Laser Scanning Instrument

Basic to the theory behind deconvolution is the diffraction pattern of light as outlined earlier. Photons emitted by a point source (the light emitted by a molecule of fluorescent marker) distribute onto a plane or a detector according to a PSF, similar to the Airy distribution of the light wave front in a conventional microscope. The PSF for any given microscope is a compound PSF influenced by all optical components: the PSF_i. Even within one instrument, each objective lens–intermediate lenses-microscope combination has its own particular PSF_i, since the numeric aperture of the objective lens is paramount. It is important to realize that the PSF_i of a confocal instrument changes every time a different objective lens is selected.

In a routine light microscope, diffraction in the *Z* direction is neglected. By contrast, in 3D reconstructions from confocal images, knowledge of the *Z* component of the PSF_i is very important. One would expect that the axial component of the PSF_i of a confocal instrument is the same as the radial component. This is not the case, however, due to the factor-2 lower resolution in the axial direction versus that in the radial direction and, surprisingly, by the presence of the pinhole. The difference between the diffraction patterns in the *XY* and *Z* directions (and thus differences between the radial and the axial components of the PSF_i) can be understood intuitively as follows. The optical axis of a microscope is aligned with the pinhole. The optical axis "cuts through" the entire thickness of the section. As a consequence, all photons emitted by structures in the section along the path of the optical axis pass the pinhole, even the photons that have been generated in planes above and below the focal plane. The consequence of this photon behavior is that the "focal plane" in a confocal microscope is not a flat plane but a deformed plane "rippled" according to the diffraction pattern of the back-projected pinhole. In this plane, the very area where the objective lens performs best, the blur in the *Z* direction, unfortunately, is at its highest

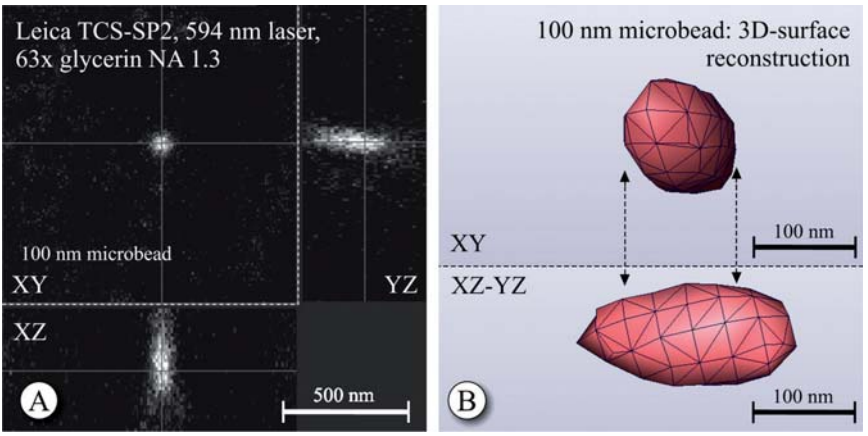

Figure 13.4. Image formation in a confocal microscope. Images of a 100-nm-diameter multifluorescent latex microsphere. (A) View of a confocal *Z*series in *XY*, *XZ*, and *YZ* directions. In the lateral direction (*XY* plane), the microsphere shows its true shape whereas in the axial direction (*XZ* and *YZ*) the microsphere appears elongated. (B) 3D reconstruction of this microsphere. The axial distortion of the sphere is caused by the different shape of the axial component of the point spread function (PSF_i) of a confocal microscope compared with the radial component.

and the confocality at its poorest. Fortunately, during scanning, the laser beam coincides only very shortly with the optical axis of the instrument. As a consequence of the presence of the pinhole, the 3D shape of the PSF_i of a confocal instrument resembles an ellipsoid rather than a sphere, with an axial or *Z* component definitely elongated compared with the radial or *XY* component (Hiesinger *et al.*, 2001; Shaw, 1995). This difference between radial and axial diffraction can easily be demonstrated by means of scanning very small fluorescent microspheres and by 3D reconstructing these spheres (Fig. 13.4, without postacquisition processing). In the *XY* plane, all microspheres appear spherical, while in the *XZ* and *YZ* planes they invariably look like mini rugby balls. The effect of the different shapes of the PSF_i measured radially versus axially is that the axial resolution of a confocal instrument is considerably lower (factor 2–2.5) than its radial resolution.

C. Key Instrument Parameters in Confocal Laser Scanning Microscopy

Since the theoretical optical considerations that hold for a conventional microscope are also valid for a confocal microscope, the key parameters to obtain high resolution in the confocal microscope are the wavelength of the light projecting through the optical system (that is, the emitted fluorescent light and not the incident light), the quality of the objective lenses (the higher the numeric aperture, the better), and the compound PSF of the optical system. Along with these factors, equipment like powerful and

reliable lasers, good beamsplitters, excellent filter sets, and highly sensitive photomultipliers are a necessity. The opinions of the manufacturers differ with respect to the size and shape of the pinhole. The back-projected size of the pinhole should match the diameter of the Airy disk belonging to the fluorescence light emitted by the specimen. The main problem here is that the emitted fluorescence falls within a spectral emission band rather than being a fixed wavelength like the laser light used for excitation. Which emission wavelength to select? Conventional wisdom here is to use the wavelength at which peak emission intensity occurs.

Manufacturers are not specific about the physical shape and size of the pinholes implemented in their instruments. The shape of the pinhole is often determined by construction-related mechanical considerations. It may be a square rather than a circular aperture. Often the position of the pinhole is fixed in the *Z* direction (also a compromise) and, when the operator switches to an excitation laser with a different wavelength, the pinhole does not change its diameter. Theoretically, the diameter of the pinhole and the distance between the pinhole and the detector plane should vary according to the wavelength, yet this seems not to deter manufacturers from designing confocal instruments with fixed-position pinholes. Like many instruments, an actual confocal instrument is a compromise between theory and the practically attainable.

Since the PSF_i determines the amount of divergence of photons on their way from the fluorescent object to the detector, an advanced deconvolution program needs to know this PSF_i to do its job properly. Each confocal instrument has its own PSF_i. Although this PSF_i depends primarily on the objective lens, as argued above, construction factors play a role as well. The PSF_i at a particular magnification can be approximated via measurements on microspheres in the actual instrument and can be used in the computer program to calculate with high-statistical likelihood the origin of the photons.

The result of deconvolution calculations is a markedly improved image. Several deconvolution algorithms exist of which we use the Huygens II professional software (SVI, Hilversum, The Netherlands, http://www.svi.nl). Versions of Huygens II exist for Unix, Linux, Apple, and Windows platforms. Huygens II rapidly deconvolves *Z* series of images. According to Kano *et al.* (1996; images obtained in a two-photon confocal instrument), an improvement in resolution by two times in the *XY* plane can be obtained as well as an improvement by four times in the *Z* direction. This could amount to a resolving power with blue light (450 nm) of structures as small as 140 nm in the radial direction and 285 nm in the *Z* direction. Since the size of a CNS axon terminal is in the 0.5–1.0 μm range, the resolution of combined confocal scanning-deconvolution is therefore sufficient to study for instance colocalization of markers in nerve fibers and axon terminals. An active zone of a synapse (200–300 nm wide, 50 nm thick), if stained with a fluorescent marker that produces enough emission to hit the detector, will be rendered as a bright aggregate of fluorescence.

III. METHODOLOGY

A. Introductory

With the above physicooptical constraints and possibilities in mind, we use the confocal microscope to acquire images at high resolution. Through subsequent postacquisition processing, we improve the resolution via deconvolution.

We will now present the methodology used in carrying out our triple labeling experiment. Two rules of thumb apply throughout the entire process. First, overall performance depends on the weakest link in the chain. Second, preacquisition histology should be perfect. The ultimate goal is to identify the presynaptic terminal via neuroanatomical tracing (marker #1), to identify simultaneously the postsynaptic element (marker #2), and a protein uniquely associated with the synapse (marker #3). The outcome is a triple immunofluorescence protocol, which we will discuss in detail in this section. This protocol is illustrated with the projection in the rat from the presubiculum to parvalbumin interneurons in the entorhinal cortex (Wouterlood *et al.*, 2003).

In the introduction, we put forward that a synapse can be represented at the light microscopic level by a presynaptic axon terminal, a postsynaptic structure, and by molecules uniquely attached to a synapse as the intermediate marker. The challenge is to visualize this three-marker sandwich. Given the small dimensions of these sandwiches, we need to go beyond the classical limit of resolution to make them visible. We approach this suboptical resolution scale by using confocal laser scanning followed up with deconvolution and 3D reconstruction. Since "breaking the resolution barrier" occurs at the very end of a long and rather complicated chain of histochemical, physicooptical, and digital procedures, one should continuously keep in mind that the quality and reliability of the final 3D reconstructed image is completely dependent on the quality of every manipulation of the tissue sections in all the stages preceding the actual confocal laser scanning session and, of course, on the parameters applied during the laser scanning and postacquisition computer processing. The weakest link somewhere in the chain immediately affects the resolution at the end of the chain.

The multitude of factors influencing the end result of any confocal experiment can be grouped into four major clusters. As many factors as possible will be discussed while we proceed with the methodology:

1. Preacquisition histological procedures.
2. The confocal instrument itself: lenses, filters, detectors, and parameters.
3. Human factors like the skill, competence, and awareness of the person operating the confocal instrument.
4. Postacquisition image processing.

Sloppy histology, poor understanding of the basics, and incompetent operation of the instrument and computers can easily ruin the results and cannot be offset by the most sophisticated instruments, computers, and postacquisition computer processing.

The ultimate goal of multiple fluorescence is to observe sandwiches of aggregates of fluorochromes. This goal can be reached only when the brain is very well fixed such that proteins have had no chance before, during, or after fixation to diffuse out or move away from their original position. From this starting point, it follows that all membranes in general, and pre- and postsynaptic membranes in particular need to be in perfect shape. The same prerequisite of a very well fixed brain also holds for studies with the confocal instrument in which one wants to analyze colocalization of multiple markers in small cellular compartments such as axon terminals. On the other hand, fixation should not be too rigid because antibodies still must be able to penetrate into the sections in order to bind to their favorite epitopes. The fixation conditions are comparable to those described for preembedding electron microscopy by Leranth and Pickel (1989) in the previous issue of this book, except that in confocal laser scanning histochemistry, the use of detergents in the incubation media is allowed as a measure to enhance the penetration of the antibodies into the sections.

B. Anterograde Neuroanatomical Tracing and Follow-Up

The chapter by Lanciego in this book summarizes the pros and cons of various neuroanatomical tracers. Our experiment aims to visualize synapses, so we need to label the presynaptic axon terminal. This is best done via anterograde neuroanatomical tracing. A versatile anterograde tracer is biotinylated dextran amine (BDA; 10 kDa, Molecular Probes, Eugene, OR). This tracer is stable, its application relatively easy, it labels all the processes of neurons and their appendages throughout, and the detection is fairly straightforward with streptavidin conjugated to a fluorochrome of choice. BDA is also highly compatible with electron microscopy (Wouterlood and Jorritsma-Byham, 1993). An alternative anterograde tracer is the lectin *Phaseolus vulgaris* leucoagglutinin (Gerfen *et al.*, 1989; Gerfen and Sawchenko, 1984; Groenewegen and Wouterlood, 1990; Lanciego, 2005, this volume; Zaborszky and Cullinan, 1989; Zaborszky and Heimer, 1989). The procedural steps are listed in the Appendix.

C. Controls

Controls are extremely important in multilabel fluorescence staining. Each stage of the entire procedure requires its specific controls:

1. Immunofluorescence controls to test the specificity of the immunostaining.

2. Confocal instrument controls to check in a multichannel configuration the specificity of each channel and, separately, to check laser alignment. The laser alignment check is especially important if the purpose is to make 3D reconstruction of small structures presumed to lie very close to each other (markers #1 and #2 in our paradigm), or if the purpose is to study colocalization of markers in small structures (markers #2 and #3 in our paradigm).

1. Immunofluorescence Specificity Controls

Inherent in immunocytochemistry is the requirement to conduct sufficient control experiments to determine the specificity of the binding of the primary antibody to its epitope, the binding of the proper secondary antibody to the proper primary antibody, to exclude cross-reactivity, and to check whether nonspecific binding of antibodies to tissue components occurs (see Leranth and Pickel, 1989). In brief, control incubations should be designed to test that the primary antibodies react only with their specific epitopes and with no other tissue component, and to check that each of the secondary antibodies–fluorochrome conjugates reacts only with its corresponding primary antibody and not with the noncorresponding primary or secondary antibody. Primary antibodies can be tested with absorption controls (see Leranth and Pickel, 1989). Various controls with fluorochrome-tagged secondary antibodies are described by Wouterlood *et al.* (1998). It is important to know a priori that the immunocytochemical reactions have been successfully completed since otherwise no firm conclusions can be drawn from the images acquired in the confocal instrument. A thorough discussion of the application of fluorochromes in a multilabel experimental environment is provided by Wessendorf (1990), although this discussion stems from the preconfocal era. However, the principles of sound immunofluorescence practice as outlined by Wessendorf (1990) are still valid for confocal laser scanning configurations.

2. Confocal Instrument Controls

Central in confocal laser scanning is the concept of a *channel*. A channel is a specific configuration of the confocal instrument, which includes illumination with one of the available lasers and the corresponding specific filter, mirror, and detector settings such that the instrument is optimized to detect the associated fluorochrome and nothing else. This is especially important in multifluorescence confocal laser scanning. Each fluorochrome should be visible only in its own channel and not in channels set up to detect other fluorochromes. Signal detected in a channel associated with a different fluorochrome is considered *crosstalk* (also known as bleeding through).

Configuration of the channels of the instrument depends on the characteristics of the used fluorochromes. Conversely, the selection of proper

fluorochromes is based on the laser wavelengths and filters available in the confocal instrument.

D. Fluorochromes and their Characteristics

The lasers used in confocal instruments produce spots of very high-intensity illumination of the section. Fluorochromes designed for use in such a harsh environment should therefore be particularly stable under high-intensity illumination. The classical fluorochrome fluorescein isothiocyanate is unsuitable in a laser illumination environment, since this dye is bleached away in a matter of seconds. Dyes with improved resistance to bleaching are the carbocyanine dyes (Amersham) and the Alexa Fluor™ dyes (Molecular Probes). Bleaching can be suppressed by the addition of an antifading agent to the mounting medium (see Longin *et al.*, 1993; Ono *et al.*, 2001).

In addition to resistance to bleaching, a fluorochrome for use in a CLSM should meet the following demands.

1. Excitation Spectrum

The shape of the excitation curve of a fluorochrome (excitation intensity plotted against wavelength) should be smooth, narrow, and steep, with an excitation maximum close to or coinciding with the wavelength of the assigned laser light of the confocal instrument. As an example, the fluorochrome Alexa Fluor™ 488 (excitation maximum at 491 nm; Table 13.1) will produce fluorescence with the highest intensity and quantum efficiency when illuminated with a 488 nm laser. Alexa Fluor™ 594 (excitation maximum of 590 nm) should be used in conjunction with a 594 nm laser. It

Table 13.1. Fluorochromes, their excitation peaks and the laser wavelength with which we excite these dyes in our confocal instruments, and potential of excitation crosstalk.

Fluorochrome	Excitation peak (nm)	Illumination with laser wavelength(s) (nm)	Excitation crosstalk with laser wavelength
Cy2™	489	488	—
Cy3™	554	543, 568	—
Cy5™	649	633, 647	—
Alexa Fluor™ 488	491	488	—
Alexa Fluor™ 546	556	543	—
Alexa Fluor™ 556	577	568	—
Alexa Fluor™ 594	590	594	—
Texas Red	595	594	568
Alexa Fluor™ 633	632 (shoulder at 580)	633, 647	568, 594
Alexa Fluor™ 647	650 (shoulder at 580)	633, 647	568, 594

Excitation peaks as provided by the manufacturers of the respective fluorochromes.

makes little sense to view fluorescence by, say, Alexa Fluor™ 594 through illumination with a laser that produces 488 nm or even 543 nm laser light. One may expect in those cases a low-quantum efficiency (a low intensity of the fluorescence related to the intensity of the excitation light, i.e., little bang for the buck and much bleaching), since the peak absorption of this Alexa dye is too far off the fixed excitation wavelengths supplied by the 488 and 543 nm laser light.

2. Emission Spectrum

Likewise, the curve of the fluorochrome showing the intensity of the emitted light plotted against the wavelength should be similarly shaped as its (ideal) excitation curve: smooth, narrow, and steep. Especially, the "tail" of the curve lingering toward the "red" end of the light spectrum should either be absent or else be as low and flat as possible. If the emission curve has an above-background spectral tail, it may cause emission crosstalk in double or multiple laser scanning, that is, inappropriate signal in channels configured toward the "red" end of the spectrum.

3. Resistance of Fluorochromes to Bleaching is Important for 3D Reconstruction

Bleaching of fluorescence signal (also called quenching or fading) may easily occur because of the very intense illumination of the fluorochrome by its assigned laser. 3D reconstructions are made on the basis of *Z* series of images. Imagine what happens if the fluorochrome offers little resistance to bleaching. The basic fact here is that the illumination part of most laser scanning microscopes is not confocal at all: the laser excites all fluorochrome molecules throughout the entire thickness of the section and all these excited molecules emit fluorescence; only *photons emitted from the focal plane* are detected. In a *Z* series, the region of interest (ROI) of the section will be exposed to a particular amount of laser light every time an image is acquired. If a *Z* series consists of n images, the ROI is exposed n times to the high-intensity laser light. In case of weak fluorescence, the operator may decide to scan each *Z* plane twice and average the result (the option *frame averaging* or *Kalman filtering*). In such a scenario, the ROI is exposed $2n$ times to the intense laser light. At the high magnification used in our experiments (63× immersion), all the laser light is concentrated by the objective lens onto a very small ROI. Thus, bleaching occurs faster at high magnification than at low magnification. In a *Z* series subject to bleaching, the first frame of the series will show a complete range of gray values. The second frame of the series may look less bright and crisp, while some low-intensity gray values will have disappeared. This reduction of brightness and contrast together with loss of low-gray values will progressively occur with the continuation of

the *Z* series until at some point the acquired frame will be entirely black (no intensity left, everything bleached). When this occurs, completion of the *Z* sectioning becomes senseless and the subsequent 3D reconstruction becomes senseless as well. Thus, the operator of the confocal instrument always needs to be aware that bleaching is a potential danger. Countermeasures against bleaching are numerous. An experienced instrument operator knows to balance these countermeasures:

1. Addition of an antifading agent to the embedding medium prior to mounting (see Longin *et al.*, 1993; Ono *et al.*, 2001). There are several good antifading agents on the market, e.g., Vectashield™ Mounting Medium (Vector Laboratories, Burlingame, CA; www. vectorlabs.com) and ProLong (Molecular Probes). One can also apply one's own homemade additive (Platt and Michael, 1983).
2. Reduction of the laser intensity and increase in the gain (sensitivity) of the photomultipliers.
3. Reduction of the number of *Z* images.
4. Increase of the *Z* stepping increment.
5. Faster scanning (produces more noise, though).
6. Reduction of the image bitmap size.
7. No averaging of images (Kalman filtering off).
8. Increase in the scanning frequency.

E. Notorious: Crosstalk

One of the phenomena that may interfere in a negative way with the results in multilabel fluorescence studies is crosstalk. Crosstalk (also called "bleeding through") is, generally speaking, the observation of inappropriate fluorescence signal in a channel configured for imaging another fluorochrome. Crosstalk classically occurs always in a "higher" channel, that is, a channel configured around a laser–fluorochrome combination with longer wavelengths. We distinguish two types of crosstalk: emission crosstalk and excitation crosstalk.

1. Two Types of Crosstalk

Emission crosstalk is the excitation of a fluorochrome by its associated laser, and the inadvertent occurrence of some emission of this fluorochrome in the next, higher channel configured for a longer wavelength fluorochrome/laser combination. When emission crosstalk occurs, the appropriate channel shows a nice image while a faint copy of the image occurs in the inappropriate, "higher" channel. An example is excitation by a 488 nm laser of the fluorochrome Alexa Fluor™ 488, producing some emission in a channel configured around the combination of 543 nm laser/Alexa Fluor™ 546 (Figs. 13.5B and 13.6).

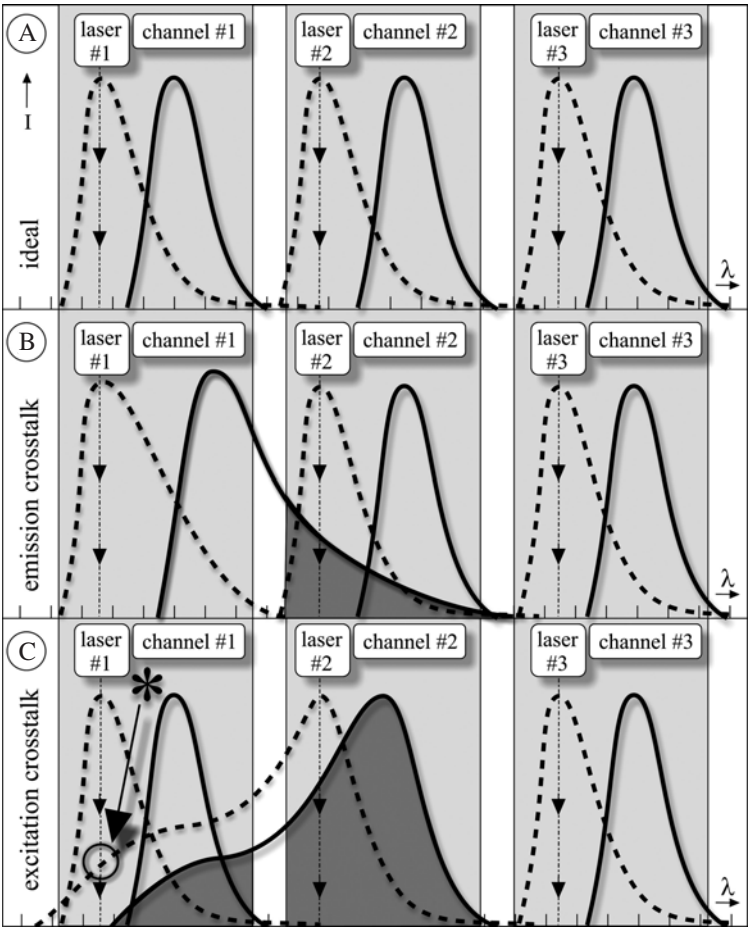

Figure 13.5. Diagram explaining channel separation and crosstalk in a confocal laser scanning instrument. Dashed line = excitation curve, solid line = emission curve. (A) Situation with ideally separated channels. For each channel, the laser excitation, fluorochrome excitation, and emission are strictly confined to the assigned wavelength frequency band. There is no interference between neighboring channels. (B) Emission crosstalk in channel #2 (shaded area): emission of the fluorochrome in channel #1 overflows in channel #2. This type of crosstalk can be avoided by sequential scanning. (C) Excitation crosstalk: the laser in channel #1 excites fluorochrome 1 but also fluorochrome 2 (emission of fluorochrome 2 in channels #1 and #2 is shown shaded), since the excitation curve of fluorochrome 2 extends into the wavelength frequency band of channel #1. This type of crosstalk cannot be avoided by sequential scanning. The signal produced in channel #1 by fluorochrome 2 has to be removed by postacquisition computer processing (so-called linear unmixing).

Excitation crosstalk is the effect in a double- (or triple-) fluorescence experiment that a particular laser excites next to "its own" associated fluorochrome also a second fluorochrome, e.g., one that belongs to the next, "higher" channel. Inadvertent signal of that next-channel fluorochrome is

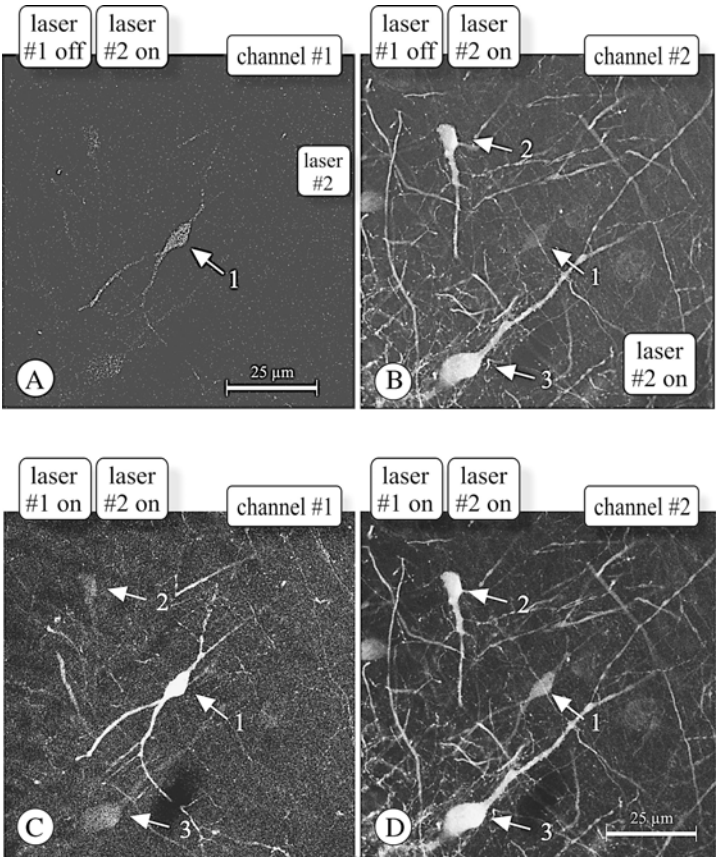

Figure 13.6. Practical examples of emission crosstalk, excitation crosstalk, and signal leakage. Section of rat hippocampal field CA1 immunostained with antibodies against calretinin (cell 1, Alexa Fluor 594) and parvalbumin (cells 2 and 3; Alexa Fluor 633). These markers were selected because CA1 cells express either calretinin or parvalbumin and never both markers. Channel #1: 594 nm laser, emission bandpass filter setting of 605–628 nm. Channel #2: 633 nm laser, emission longpass filter setting of 643–750 nm. The detector sensitivity for both channels had been optimized for its corresponding signal and was not further changed. Image pair A and B: Situation with only the laser in channel #2 switched on. In both channels, a ghost of the calretinin cell 1 is visible. In channel #1, this signal leakage effect is probably due to internal reflections or by incomplete cutoff by the bandpass filter assigned to channel #1. In channel #2, the ghost is caused by excitation and emission of the 594 fluorochrome by the 633 nm laser. The image pair in C and D was recorded with both lasers switched on. In C, ghost images of the parvalbumin cells 2 and 3 are visible caused by excitation crosstalk: the 594 nm laser excites the Alexa Fluor™ 633, and signal is picked up in channel #1. The ghost of the calretinin cell 1 in channel #2 is caused by emission crosstalk or by straightaway excitation of Alexa Fluor™ 594 in channel #2. All images at the same magnification.

produced in both channels. A faint copy of the image in the second channel is produced in the first channel, in addition to the image appropriate for the first channel. This "excitation" crosstalk signal resembles emission crosstalk, yet has a completely different cause (Fig. 13.6). Excitation crosstalk is much more difficult to recognize and avoid than emission crosstalk. An example is the excitation of Alexa Fluor™ 633 (emission in both 594 and 633 nm channels) by a 594 nm laser used to excite the fluorochrome Alexa Fluor™ 594 in the 594 nm channel (Figs. 13.5C and 13.6).

In addition to crosstalk phenomena, there may be internal reflections in the confocal instrument and incomplete cutoff of bandpass filters producing ghost images into a lower channel ("signal leakage"), e.g., signal of a "red" fluorochrome into a "green" channel (Fig. 13.6A).

2. Procedure to Determine Emission Crosstalk

Although it is possible to determine this type of crosstalk in double- or triple-stained sections, this check is best done with single-stained sections: for each channel, a section stained only with the fluorochrome assigned to that particular channel. In our laboratory, we have within reach these single-stained control sections for each of the laser excitation wavelengths with which our confocal instrument is equipped. In this check, we submit to the test three single-stained sections, each associated with its own channel of a three-channel setup.

1. Use the three single-stained sections to configure, one after another, three channels such that on the display screen a nice and brightness-contrast balanced image appears for each individual channel. Save these settings.
2. Insert the single-stained section associated with the first channel in the microscope.
3. Turn the laser intensities for the second and third channels back to zero but *do not change* the detector sensitivities for these channels.
4. Illuminate the section subsequently with the laser belonging to the first channel only (e.g., 488 nm).
5. Images remaining in the second and third channels represent emission crosstalk.
6. Repeat this procedure for the next combination of channels.

A countermeasure against emission crosstalk is to reduce the intensity of the laser in the first channel such that the crosstalk image in the second channel is no longer visible (of course, the laser for the second channel should be turned down temporarily to see the effect). Adjust, if necessary, the detector sensitivity for the first channel. Repeat the procedure for the next combination of channels: two and three (do not increase at this stage the sensitivity setting of channel 2, since the current setting of that channel

has been determined in order to avoid crosstalk from channel 1). Next, continue multichannel laser scanning with these settings for laser intensities and detector sensitivities. If these measures do not help, then sequential scanning might offer a solution. Emission crosstalk can be avoided completely by resorting to a sequential scanning procedure.

In a multichannel configuration, crosstalk usually occurs in "higher" channels, for instance, crosstalk showing up in a 543 nm channel when the laser in the other channel is a 488 nm laser. This (emission-type) crosstalk occurs because the emission spectrum of any fluorochrome is always shifted to longer wavelengths compared with the excitation spectrum (so-called *Stokes shift*) and never to shorter wavelengths (which is impossible according to the second law of thermodynamics). The "sneaky" feature of excitation crosstalk is that it occurs in a channel configured around a shorter laser wavelength (a "lower" channel) than its appropriate channel. Given Stokes shift, this sounds paradoxical at first sight. There is, however, no conflict with the second law of thermodynamics at this point. The essence of this type of crosstalk is that the involved fluorochrome is excited by the laser belonging to the inappropriate, "lower" channel and that it produces its normal, Stokes-shifted fluorescence signal in both the inappropriate channel and the appropriate channels.

Excitation crosstalk is much harder to detect than emission crosstalk. Also, because most microscope operators trained as they are in recognizing Stokes shift and associated emission into a higher channel do not expect crosstalk in a "lower" channel, they are inclined to be aware of and test only for emission crosstalk and not for excitation crosstalk. Excitation crosstalk can be considerable when, for example, the fluorochrome Alexa Fluor™ 594 (excitation 594 nm laser) is combined with Alexa Fluor™ 633 (excitation 633 nm laser). The excitation curve of the latter fluorochrome possesses a shoulder that makes the dye sensitive to excitation at 594 nm. As a consequence, Alexa Fluor™ 633 produces signal simultaneously in both the 594 and 633 nm channels when the section is illuminated with 594 nm laser light (Figs. 13.5C and 13.6). Similarly, excitation crosstalk occurs for instance at 568 nm laser illumination with the combination Cy3™ (568 nm excitation maximum)–Alexa Fluor™ 633 (633 nm excitation maximum). It occurs also at 568 nm laser illumination with the combination Cy3™ (568 nm excitation maximum)–Alexa Fluor™ 647 (633 nm excitation maximum).

3. Procedure to Determine Excitation Crosstalk

This check is done with double- or triple-stained sections, with backup of single-stained sections. The test cannot be done with markers that are colocalized. Prior to testing, the single-stained sections should be tested to be sure that the individual fluorochromes do not produce emission crosstalk.

In this example, it is assumed that excitation crosstalk occurs in two adjacent channels:

1. Configure with a double-stained section two adjacent channels such that on the display screen a nice, brightness–contrast balanced image appears for each channel. Save these settings.
2. Replace the double-stained section with a single-stained section containing only the fluorochrome assigned to the *second* channel.
3. If now in the first channel an image is detected, this is due to excitation of the second channel's fluorochrome in the first channel. Increasing and decreasing the laser intensity for the first channel increases and decreases the amount of this excitation crosstalk, respectively.
4. Repeat these steps for the next combination of channels.

Note that this check is meant only to determine whether excitation crosstalk exists in the specimen. The elimination of excitation crosstalk is quite another story since, besides the fact that excitation crosstalk is hard to detect, one cannot filter to eliminate this type of crosstalk. Scanning in sequential mode offers no solution either since both fluorochromes are excited and produce emission whenever the first laser illuminates the specimen. The only way to get rid completely of excitation crosstalk is to replace the "offending" fluorochrome with a completely different fluorochrome. A way to intentionally reduce excitation crosstalk is via postacquisition image processing by a program called "dye separation" or "linear unmixing," provided that the intensity of the crosstalk signal is modest.

There exist several laser-fluorochromes combinations, which are relatively safe with respect to excitation crosstalk. Of course, these combinations should match the available lasers and filters of the confocal instrument. The bottomline is that with any combination of fluorochromes, the spectral excitation curves must be as much separated from each other as possible (as in Fig. 13.5A).

Examples of such "safe" combinations are the following:

1. Double-fluorescence labeling

1st laser (nm)	1st fluorochrome	Combined with	2nd laser (nm)	2nd fluorochrome
488	Cy2™		568	Cy3™
488	Alexa Fluor 488		568	Alexa Fluor™ 568
488	Cy2™		594	Alexa Fluor™ 594
488	Cy2™		594	Cy5™
488	Cy2™		647	Cy5™
488	Alexa Fluor™ 488		647	Alexa Fluor™ 594
488	Alexa Fluor™ 488		647	Alexa Fluor™ 647
488	Alexa Fluor™ 488		647	Alexa Fluor™ 647
488	Alexa Fluor™ 488		647	Cy5™

2. Triple-fluorescence labeling

1st laser (nm)	1st fluorochrome	Combined with	2nd laser (nm)	2nd fluorochrome	Combined with	3rd laser (nm)	3rd fluorochrome
488	Cy2™ or Alexa Fluor™ 488		543	Alexa Fluor 546		594	Alexa Fluor™ 594
488	Cy2™ or Alexa Fluor™ 488		543	Alexa Fluor 546		647	Alexa Fluor™ 633 or 647
488	Cy2™ or Alexa Fluor™ 488		543	Alexa Fluor 546		647	Cy5™

4. Practical Advice to Guard Against False Results Caused by Crosstalk

1. Always be aware of crosstalk.
2. Keep single-stained sections at hand.

When a particular set of scanning parameters for multifluorescence scanning has been determined such as laser intensities, detector sensitivities, filter selection, etc., first scan single-stained sections with these parameters and check whether an image is produced in the inappropriate "higher" or "lower" channels.

F. Operating the Confocal Instrument: "Operator Awareness"

A CLSM is a complicated optical and digital instrument, and a thorough understanding of what one is doing and what is happening (in physicooptical terms and in terms of instrument handling and software) is necessary. The reason is that by simply turning the controls of the instrument always some image can be produced in which the information contained may range from doubtful to completely worthless. The operator should always keep in mind that images obtained should represent the real world as close as possible and that the imaging should not be disturbed by some interference such as false positivity (e.g., channel crosstalk, sensitivity too high) or false negativity (e.g., out of focus, incorrect filter selection, sensitivity too low, fading, insufficient penetration of fluorescent marker). As the software in new confocal instruments is increasingly being equipped with all sorts of automatic functions, chances are on the rise that an unaware or inexperienced operator working "on autopilot" may program the detectors to acquire invalid or noninformation instead of a valid series of images.

In an instrument equipped with separate lasers, the perfect alignment of these lasers is a matter of concern. In a multiuser environment, instrument awareness of the operator is necessary at this point. Alignment and/or chromatic aberration can be tested with multifluorescent latex microspheres (e.g., the TetraSpeck® microspheres kit, Molecular Probes) or with sections containing small structures multilabeled on purpose (Wouterlood *et al.*, 1998). Also, for the purpose of calibration, we have control brain sections

at hand containing axons labeled anterogradely with the neuroanatomical tracer BDA and incubated with a cocktail of streptavidin conjugates: Alexa Fluor™ 488, 546, and 633. By virtue of this triple-color cocktail, the same labeled fiber fluoresces under illumination with the 488, 543, or 633 nm lasers. In the confocal instrument, we scan in three channels and we overlay the acquired images. If misalignment or chromatic aberration occurs, this will reveal itself as "pixel shift," which is the slight deviation of the image in one channel compared with that acquired in a different channel. Note that in addition to radial pixel shift (in the *XY* plane) also axial pixel shift may occur (in the *XZ* and *YZ* planes). We use our triple-stained calibration sections to investigate both radial and axial pixel shifts (Fig. 13.7; see below for further details on pixel shift and image mismatch). The advantage of our calibration sections is that the labeled fibers are embedded in brain tissue. The brain parenchyma surrounding the fluorescence-marked structures is by no means isotropic. This anisotropism may cause distortion of the image. In this respect, our calibration sections are more realistic than slides containing multifluorescent latex microspheres embedded in an ultrahomogeneous, isotropic mounting medium.

G. Postacquisition Image Processing and 3D Reconstruction

Image processing software is available from a range of companies. Several manufacturers of confocal instruments offer a dye separation (linear unmixing) package to improve spectral separation if necessary. We prefer perfect signal separation at acquisition time, though, before relying on postacquisition dye separation. We consider the latter a measure of last resort.

Dye separation attempts, and often succeeds, in removing emission crosstalk from the acquired images. These programs use the spectral emission characteristics of the fluorochromes. As mentioned earlier, a nasty characteristic of the fluorochrome Alexa Fluor™ 633, and the same holds also for Cy5™, is that its excitation spectrum has a shoulder at 568 nm. This implies that these fluorochromes always produce fluorescence when a 568 nm laser is used (excitation crosstalk in the 568 nm channel, cf. Fig. 13.6) and that these fluorochromes under 568 nm laser illumination produce signal as well in the 633 nm channel, even when the 633 nm laser is switched off. When it is impossible in such and similar cases to use different fluorochrome combinations, then postacquisition dye separation is indicated as a helpful tool to remove the unwanted results of excitation crosstalk.

1. Deconvolution

As argued in the theoretical part of this chapter, the quantum physics of image formation predicts that any image recorded with an optical instrument is always blurred to some degree. The amount of blur depends on the

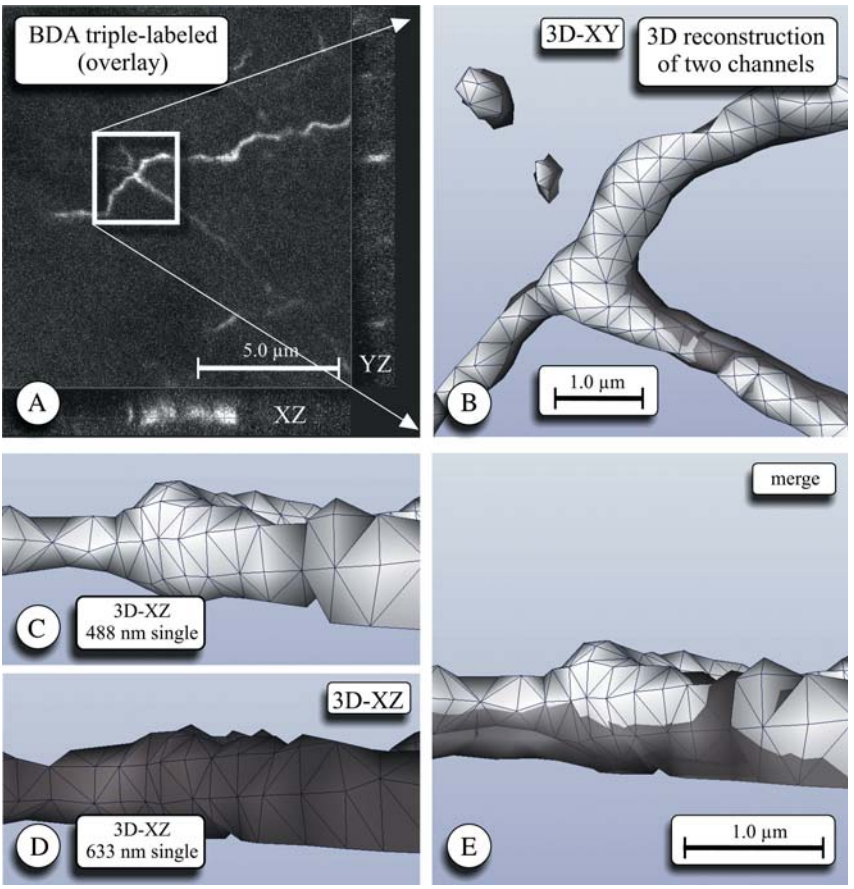

Figure 13.7. Pixel shift and image mismatch. Imaging of a BDA-labeled fiber stained with a cocktail of three fluorochromes. Image series not deconvoluted. (A) Composite *XY*, *XZ*, and *YZ* view of the image series. In the color image, shift of green and red pixels is seen in the axial direction; there is no shift in the lateral direction. (B) Enlarged portion of (A) 3D reconstructed (two of the three channels, *XY* view). There is no lateral shift of both images indicating that radial alignment of the lasers is perfect. (C, D) Single-channel 3D reconstructions of the image in the 488 and 633 nm channels (3D reconstruction turned 90°; *XZ* view). (E) Merge of C and D showing that in the axial direction, there is image mismatch. In this case, mismatch amounts to ~100 nm.

objective lense i.e. it is instrument specific information about how blur in a particular optical instrument is produced. This characteristics can be used to calculate from a blurred image via a statistical approach an image that resembles the original object with the highest degree of confidence. This reversal of the process of image formation is called deconvolution, "deblurring," or "image restoration" (Bertero *et al.*, 1990; Snyder *et al.*, 1992; van der Voort and Strasters, 1995). Deconvolution is the final step breaking the resolution limit barrier. Alternatively, deconvolution can be applied when an optical

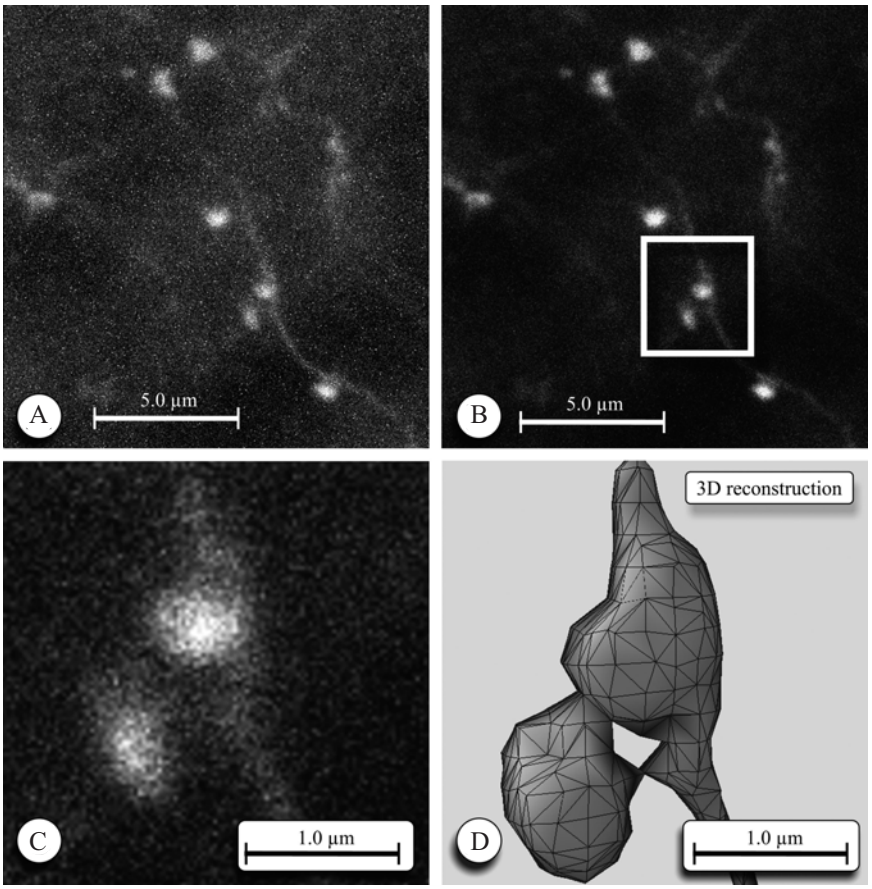

Figure 13.8. Deconvolution of a Z series of images of a BDA-labeled fiber. (A) Composite image of the Z series immediately after acquisition. (B) Same image series, deconvoluted with Huygens II software. (C) Detail of B. (D) 3D reconstruction of the detail in C.

signal is particularly blurry or noisy. Several deconvolution algorithms exist: blind deconvolution, iterative deconvolution according to Miller–Tikhonov, and iterative maximum likelihood estimate (MLE) deconvolution. MLE is specifically advised for the deconvolution of Z series of confocal images. The core of MLE consists of a statistical calculation that takes into account the PSF_i of the confocal instrument. The characteristics of the objective lenses and the other optical parts of the confocal instrument used for image acquisition, as well as the refractive indices of the tissue, immersion and embedding media, contribute to this PSF_i. The computer program uses the PSF_i to calculate, for each pixel of each acquired image in a Z series, the statistical likelihood of the exact origin of the photons emitted by the fluorescent specimen. The result is a statistically reliable, improved version of the Z image series (Fig. 13.8). The deconvolution program used in our laboratory can, however, only process the Z series of images belonging to one

channel at a time, and so we have to run the program as many times as there are channels. After deconvolution, the *Z* series of the respective channels can be merged into a final multicolor image in which all immunostained structures are visible, color-coded according to their specific microscope channel. The increase in resolution can be as much as two times in the radial direction (*XY*) and four times in the axial direction (*Z*) (Kano *et al.*, 1996; this holds for two-photon confocal images).

Note that a multicolor 3D reconstruction is in fact an overlay of as many separate 3D reconstructions, one for every channel in the confocal instrument. For instance, a three-channel confocal imaging session produces three *Z* series of images. Each of these series is deconvoluted on its own and then merged into one final 3D reconstruction. The color code assigned to each single-channel reconstruction is conserved. Most operators of confocal instruments adhere to the convention to render the 3D reconstruction in the first channel in green, in the second channel in red, and that in the third channel in blue. The color of the fluorescence emitted by the fluorochrome is used as the associated color in the 3D reconstruction. This convention has of course nothing to do with the real colors since all confocal images are basically 8- or 12-bit gray scale bitmapped images.

2. Correction for Image Mismatch

Because in a multilabel experiment the images acquired in each channel are 3D, reconstructed independently from those acquired in the other channels, small deviations of the relative positions of reconstructed objects could go unnoticed. This so-called image mismatch is a source of both false positivity and false negativity when it comes to the detection of sandwiches of three (independently reconstructed) markers (Wouterlood *et al.*, 2002). Here, the intentionally triple-stained, single tracer containing sections comes back into focus (Fig. 13.7). The 3D reconstructions in each channel of the fibers in these sections should exactly match. If, for example, the 3D reconstructed image in one channel for some reason does not match with those in the two other channels, this is evidence that somewhere in the chain of image acquisition and processing something has gone wrong. The cause may be laser misalignment, deviation of the scanning mirrors, chromatic aberration, operator unawareness, and so on.

In each confocal image acquisition session we scan, for the purpose of instrument calibration, always a preparation containing intentionally triple-labeled fibers. The 3D reconstructed images of these fibers are used to detect image mismatch. If necessary, we can correct image mismatch by shifting the 3D reconstructions in each channel a few pixels in the appropriate *X*, *Y*, or *Z* direction. The result of this exercise is that in 3D reconstruction, the perfect overlay image of the triple-stained fibers appears like a structure painted with three layers of paint of different color. The amount of necessary shift is the correction factor that is next applied to the *Z* series of the images belonging to the scientific experiment. One assumption underlying this correction is

that the parameters of the confocal instrument causing the misalignment are constant during the entire image recording session. Another assumption is that these parameters are similar for both the calibration section and the sections belonging to the scientific experiments.

Most confocal instruments are used in a multiuser environment. It is relevant in such an environment to conduct every now and then a check of the instruments to see that the alignment of the lasers and other components has not changed over time. It should also be noted that mismatch may occur in a confocal instrument just after switching on (a "cold" instrument), and then decrease until it becomes stable (in our instrument, a plateau is reached 30 min after powering on) (Wouterlood *et al.*, 2002).

3. Multichannel 3D Reconstruction

There are several competing software packages on the market capable of doing the job of calculating and rendering 3D reconstructions. In our laboratory, we have installed two packages: FluVR™ (SVI) and Amira™ (www.amiravis.com), which both run on the same Silicon Graphics workstation as the deconvolution software does. FluVR™ is a so-called volume-rendering program, whereas Amira™ is a surface-rendering program. Versions of both programs are available running under the Linux and Microsoft Windows® operating systems.

- *Volume rendering*: In this type of 3D rendering, a *Z* series of images is considered as a rectangular box filled with layers of cubes. Each layer corresponds with one frame of the image series. Each of the cubes (a voxel) has an assigned gray value. The program considers the gray value of each voxel as a measure for the absorption and emission of light by that voxel, and it starts a simulation in which it casts light from a virtual light source onto the space filled with voxels. Next, the program calculates the amount of light absorbed and the amount of fluorescence emitted by each voxel (depending on their gray value). A number of parameters such as distance from the light source, direction of the light, light intensity, transparency of voxels for excitation light, transparency of voxels for emission light, angle of inspection (camera position), and even reflection from the background can be modified interactively. The result of the calculation is a simulated 3D image of the fluorescence of all voxels of the *Z* series. Since all voxels including those that are "transparent" are involved, this type of rendering produces scientifically most valid 3D reconstructions. Since volume rendering includes calculations on all voxels of the entire *Z* series, it is time and memory resource consuming. Real-time rotation of 3D structures reconstructed via volume rendering is not possible on our computer. Multichannel volume rendering is possible (up to 32 channels, SVI; personal communication).
- *Surface rendering*: In this type of 3D rendering, a *Z* series of images is also considered as a rectangular box filled with layers of grayish cubes.

However, the operator selects a particular gray value (a threshold; in 8-bit images, there are 256 possible gray values). The program calculates lines connecting all voxels in the voxel space expressing the threshold gray value and draws on screen a wireframe consisting of these isolines (expressed as a grid of triangles). The software thus connects voxels in all the three directions. The surfaces of the wireframes are covered with a colored texture of choice. All further calculations are done with the coordinates of the corners of the triangles forming the wireframe. This saves a tremendous amount of processor resources. Surface rendering allows real-time rotation and zooming. These features are also available in the PC/Windows version of the program we use (Amira™, a high-end graphics board in the PC is recommended). Surface rendering has its analog in 3D computer games, where the objects or characters are based on wireframes clad with textures. Note that, apart from the use of RGB color images as textures, the number of colors that can be assigned to these animated characters is virtually infinite. The number of channels that can be rendered in surface rendering is therefore also virtually infinite.

IV. RESULTS

After surface 3D rendering of structures containing the three markers—presynaptic marker BDA (fluorochrome Alexa Fluor™ 546, laser 543 nm), postsynaptic marker parvalbumin (fluorochrome Alexa Fluor™ 594, laser 594 nm), and synapse-associated marker ProSAP2/Shank3 (fluorochrome Alexa Fluor™ 488, laser 488)—we noted consistent spatial separation of the reconstructed immunofluorescent material. Most reconstructed ProSAP2/Shank3 aggregates appeared exterior to BDA-labeled fibers. ProSAP2/Shank3 aggregates frequently resided in the interior of cell bodies and dendrites of parvalbumin-stained cell bodies and dendrites. In accord with the expectations (localization in the postsynaptic density), ProSAP2/Shank3 material mostly had a peripheral localization in parvalbumin-labeled structures, that is, just below the surface envelopes of parvalbumin-stained structures. There were no small ProSAP2/Shank3 aggregates seen deep in the interiors of parvalbumin-expressing structures or in BDA-labeled fibers and axon terminals.

In several cases where varicosities on BDA-labeled fibers appeared to be apposed to parvalbumin immunofluorescent dendrites, we noted ProSAP2/Shank3 immunofluorescent material sandwiched in between, immediately subjacent to the surface envelope of the target neuron, or immediately next to the apposition. We regard such a sandwich as the confocal analogon of a terminal bouton, forming a synapse with the parvalbumin-containing cell body. An example of such an apposition with aggregation of ProSAP2/Shank3 immunofluorescent material in a position inside a parvalbumin cell body facing a varicosity on a BDA-labeled fiber is shown in Fig. 13.9.

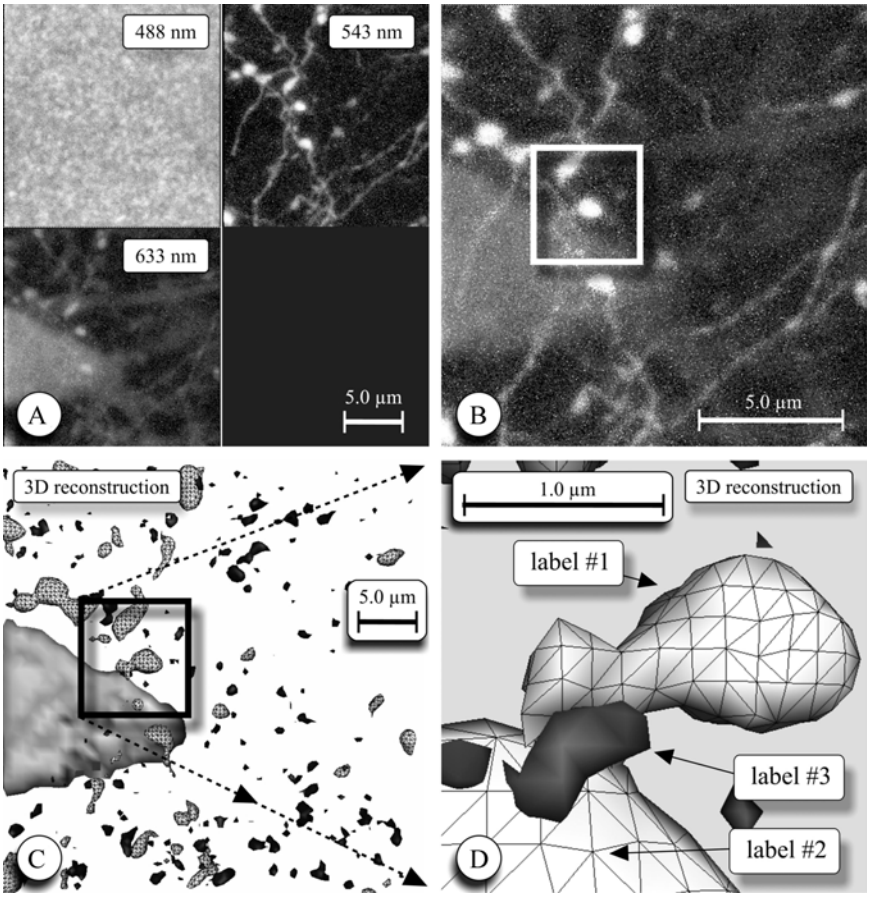

Figure 13.9. Result of triple channel confocal laser scanning, deconvolution, and 3D reconstruction. (A) Three-channel image generated by the confocal instrument of a *Z* series: ProSAP2/Shank3 (channel #1, 488 nm, label 3), BDA (channel #2, 543 nm, label 1), and parvalbumin (channel #3, 633 nm, label 2). (B) Channels #2 and #3 in overlay projection at higher magnification. BDA-labeled fibers stand out; the parvalbumin labeling is weak. (C) 3D reconstruction with Amira after deconvolution, channels merged. (D) Detail of the 3D reconstructions, showing a sandwich of the three markers indicative for a synaptic contact between the BDA-labeled fiber and the parvalbumin neuron. Label-2 structures (parvalbumin) rendered with a transparent texture.

V. CONCLUSIONS AND FUTURE

The above results of observable sandwiches of fluorescence material associated with an anterograde tracer, a postsynaptic marker, and a marker unique for a synapse lead to two conclusions. First, in this way at least appositions between processes of neurons can be made visible with great detail. Second, the application of the third marker provides the evidence in favor

of the existence of a synapse. It is, in particular, the sandwiching that proves that a synapse occurs between the labeled presynaptic axon terminal on the one hand and the structure containing the postsynaptic marker on the other. Resolution indeed seems to be sufficient to distinguish structures with sizes in the order of 0.2–0.3 μm and to see whether there is apposition and/or colocalization at this edge of the theoretically possible resolution. In a separate series of experiments, we have conducted double staining, i.e., we labeled presynaptic fibers and axon terminals with BDA and we labeled presumed postsynaptic dendrites via filling through pericellular application of Neurobiotin™. We reconstructed numerous appositions of BDA-labeled axon terminals and dendrites containing Neurobiotin. In parallel electron microscopy experiments, we lesioned the source area in the brain and we studied the area with Neurobiotin-filled dendrites at high magnification under the electron microscope. We indeed noted synaptic contacts between degenerating axon terminals and containing dendrites (Wouterlood *et al.*, 2004).

At present available in the form of antibody against ProSAP2/Shank3 is only a marker for NMDA-regulated synapses, i.e., glutamatergic, excitatory synapses. Several antibodies have been developed against components of GABAergic, inhibitory synapses, of which the $GABA_A$ receptor scaffolding protein gephyrin (Sassoë-Pognetto and Fritschy, 2000) may be a candidate for labeling experiments similar to those presented in this chapter. In that case, we could in the future map on CNS neurons, the relative numbers of excitatory and inhibitory synapses with unprecedented speed.

VI. ADVANTAGES AND LIMITATIONS

The advantages and simultaneously the disadvantages of the confocal approach as outlined in this chapter are closely associated with the ability of the combination of confocal instrument and postacquisition processing to improve resolution of an optical system down to and slightly over its very limit as governed by the physical laws of optics and diffraction of light. Resolution offered by conventional double-label epifluorescence microscopy is limited due to the great depth of focus (fluorescence emitted by structures throughout an entire section reaches the eye) and, in association with this, the low resolving power. In fact, resolution offered by conventional fluorescence microscopy is barely sufficient to determine with confidence colocalization of markers in neuronal cell bodies. Determination of colocalization of markers in fibers is out of question. Resolving power is markedly improved in the CLSM. Combination of confocal microscopy with postacquisition deconvolution further improves the total resolution to a degree that colocalization of markers in fibers and axon terminals can be determined. Furthermore, with the addition of 3D reconstruction the observer can see rapidly and decisively whether axon terminals of a particular origin or chemical signature appose presumed postsynaptic structures, for instance processes belonging

to a particular chemical category of neurons. The 3D computer reconstruction is essential here because it enables us to look at the apposing structures at any desired angle. By rotating and inspecting the 3D reconstruct, falsepositive apposition can be distinguished from true apposition because at angles of inspection different than the conventional, fixed orthoscopic look, spatial separation of the involved structures is rapidly detectable. In addition to this, the ProSAP2/Shank3 marker indicates whether there is a synaptic interface between the presynaptic terminal and the postsynaptic structure. Compared with double- and triple-labeling electron microscopic analysis, this means an enormous advantage in speed of analysis as well as in the number of synapses that can be inspected and counted in a given amount of time.

One disadvantage of the present approach is that we need more, better, and stable synapse markers, for instance a reliable marker associated with specific proteins present at the interface in inhibitory synapses. We assume that in the future, these markers will become available as the molecular structure of the postsynaptic density becomes better understood. A second and more fundamental disadvantage is that determination of synapses requires resolution at a level, which is at the edge of resolution attainable with optical systems. Note that the optical resolutions calculated in this chapter are ideal resolutions. In the extremely heterogeneous environment offered by brain tissue, the practical attainable resolution is always lower. Furthermore, the physical law of diffraction predicts that at the magnification necessary to pinpoint synapses, all stained "structures" will appear as blurry distributions of photons rather than the crisp images we are familiar with at low magnification. At a synapse, the pre- and postsynaptic markers are by nature extremely close. This, and the fluorescence associated with the synaptic marker sandwiched in between, causes overlapping distributions of photons in the detectors of the confocal microscope. This may cause confusion in many interpreters. If a crisp image is really necessary, then the electron microscope with its superior resolution (measured in tenths of nanometers instead of hundreds) is the instrument of choice. After all, electrons cannot be beaten as vehicles for the imaging of nanostructures.

APPENDIX

A. Surgery, Injection of BDA in the Rat

1. Anesthetize the rat deeply with an intraperitoneal injection of a mixture of four parts Ketaset (ketamine; 1% solution; Ket, Aesco, Boxtel, The Netherlands) mixed with three parts Rompun (xylazine; 2% solution, Bayer, Brussels, Belgium) (1 ml/kg body weight of this mixture).
2. Mount the animal in a stereotaxic frame.
3. Expose the skull and anesthetize the periost with lidocaine (10% spray; Astra Pharmaceutica BV, Zoetermeer, The Netherlands).

4. Drill an opening in the skull at the desired *X–Y* coordinates and open the meninges.
5. Lower the tip of a borosilicate glass micropipette filled with tracer (BDA, 5% in 10 mM phosphate buffer, pH 7.25, pipette tip diameter 10–20 mm) to the desired rostrocaudal, lateral, and vertical coordinate.
6. Apply to the micropipette a positive pulsed 5 mA DC current (7 s on/7 s off) for 10–15 min. Leave the pipette in situ for 10 min after delivery of the tracer.
7. Retract the pipette, close the wound, and allow the animal to recover. The survival period postsurgery is usually 1 week.

B. Perfusion-Fixation, Sectioning, Storage

1. Inject an overdose of sodium pentobarbital (Nembutal, Ceva, Paris, France; intraperitoneally, 60 mg/kg body weight).
2. Perfuse transcardially, first with 100 ml of physiological saline solution of 38°C, pH 6.9, immediately followed by 1000 ml of 4% freshly depolymerized paraformaldehyde and 0.1% glutaraldehyde in 125 mM phosphate buffer, pH 7.4 (room temperature). We use a perfusion system driven by compressed air, which delivers perfusion fluids at a constant, controllable hydrostatic pressure (Jonkers *et al.*, 1984). The thoracic aorta is clamped to ensure that all fixative is directed at the upper part of the body.
3. Immediately after perfusion carefully remove the brain from the skull. Cut 120-μm-thick slices with a vibrating microtome and collect these in chilled 125 mM phosphate buffer, pH 7.4 (vials kept on melting ice).
4. Infiltrate the slices with a cryoprotectant consisting of 20% glycerin and 2% DMSO in 125 mM phosphate buffer, pH 7.4 (Rosene *et al.*, 1986).
5. Transfer the slices to storage vials and place these in a freezer (−20 or −40°C) for later use.
6. Resection the slices into sections prior to immunohistochemistry for the purpose of obtaining better penetration of antibodies.

C. Resectioning Slices into Sections to Obtain Better Penetration of Antibodies

The third label in our paradigm (see Fig. 13.1) identifies a component uniquely associated with the synapse. We screened for this purpose many antibodies directed at protein components of receptor scaffolding molecules located in or at the postsynaptic density of the synapse. Although these antibodies work well in cell cultures, the vast majority of them suffer from insufficient penetration into brain sections of regular thickness (25–40 μm) or even worse, they simply do not penetrate at all. An antibody that works in our free-floating section incubation environment was raised against the

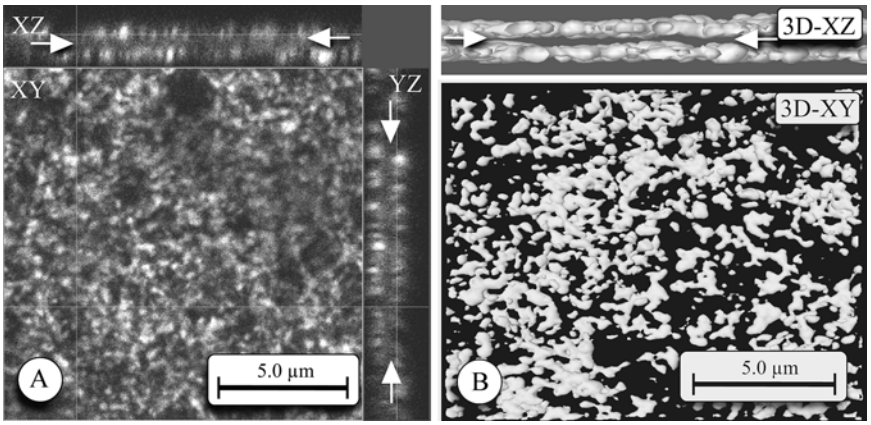

Figure 13.10. Insufficient penetration of antibodies into a section detected via *Z* confocal scanning. The marker is vesicular glutamate transporter 1, which is present in glutamatergic axon terminals. Image taken in stratum radiatum of CA1, hippocampus, 63× immersion lens NA 1.3, electronic zoom 8×. (A) Top and side views of a *Z* image stack (26 frames). Inspection of the series in simultaneous *XY*, *XZ*, and *YZ* rendering reveals intense staining of aggregates of immunofluorescence at the upper and lower surfaces of the section, while a band in its core is dark, with weak or low immunofluorescence (arrows). (B) 3D reconstruction of this *Z* series in *XY* and *YZ* view. The (artifactual) absence of staining in the core of the section (arrows) is even more dramatic after reconstruction.

protein PsoSAP2/Shank3 by Böckers *et al.* (1999). This protein is interpreted as an anchoring protein of the NMDA receptor at excitatory synapses, and it is located in the postsynaptic density (Böckers *et al.*, 2002). However, in pilot incubations, the penetration of this antibody appeared to be insufficient. The degree of penetration of an antibody can easily be measured in a confocal microscope by means of a *Z* scan of the complete section, from the upper to the lower surface (Fig. 13.10). A condition is that the marker is known to be distributed homogeneously throughout the area of interest. If in this *Z* scan, the distribution of the immunofluorescence occurs only at the outer surfaces of the section, or when the intensity of staining shows a gradient with good staining in a small superficial band at the upper and lower surfaces of the section and poor or no staining in between (as is visible in Fig. 13.10), then it is likely that penetration has been inadequate. Another phenomenon may lead to similar insufficient staining, notably a very high concentration of epitope in the section. The abundancy of epitope may lead to premature exhaustion of the antibody solution such that at a certain point no antibody is available to bind with epitope in the center of the section. Thus, a gradient type of immunostaining is produced similar to the poor-penetration type. The poor penetration phenomenon is different from bleaching caused by laser illumination since insufficient penetration shows up at both the upper and lower surfaces of a section, whereas bleaching produces a local loss of immunofluorescence throughout the section's thickness.

Several measures can be introduced to improve the penetration of antibodies or, for that matter, to attempt avoiding gradient types of immunostaining:

1. Prolong the incubation.
2. Incubate at a higher temperature.
3. Increase the concentration of antibody.
4. Reduce of the number of sections per incubation well.
5. Use less and/or smaller sections (if the epitope is present in such excess that the antiserum is fast exhausted, e.g., in case of neurotransmitters, transporters, postsynaptic density proteins, etc.).
6. Use thinner sections or sections cut on a cryostat.
7. Treat the sections with microwaves prior to or during incubation.
8. Add (excess) detergent.
9. Freeze-thaw the sections prior to incubation. This freeze-thawing is done by immersing the sections in a bath of isopentane that, in turn, is subsequently rapidly cooled down by liquid nitrogen (details in Wouterlood *et al.*, 1993).

As cryostat sections usually need on-slide incubation with antibodies, we resorted in the case of ProSAP2/Shank3 to the solution of cutting the thinnest sections possible. In order to do so, we started with 120-μm-thick slices. Slices with such a thickness (or thicker slices, e.g., 150 μm) are easy to cut with a vibrating microtome as well as easy to handle, manage, and store in a cryoprotection solution in a freezer. When needed, a 120-μm slice can be recovered from the freezer and resectioned according to the following procedure.

D. Preparation of Thin Sections for Free-Floating Incubation

1. Drip 30% sucrose on the cold stage on a freezing microtome until a mound is formed.
2. Flatten this mound by moving the knife of the microtome over it.
3. Take the 120 μm slice from its cryoprotectant and dip fast in 30% sucrose.
4. Place the 120 μm slice on a (gloved) finger and put it on the flat surface of the mound.
5. Allow to equilibrate, trim if necessary, and cut 10–15-μm-thick sections. Collect these sections in wells of a 24-well plate for further processing.

E. Triple-Fluorescence Staining Procedure

Continuous gentle agitation on a rocking plateau is always provided during the incubation to prevent the contents inside the wells from settling onto the bottom.

In between all incubation steps, the sections are thoroughly rinsed with incubation buffer: 50 mM Tris/HCl buffer with 0.875% sodium chloride, 0.5% Triton X-100, pH 8.0 (TBS-TX). We use excess of antibody solution. Steps are as follows:

1. Preincubate 1 h at room temperature with 5% normal goat serum.
2. Incubate for at least 48 h at 4°C with a cocktail of primary antibodies: mouse anti-parvalbumin (Sigma, St. Louis, MO; 1:500, marker #2) and guinea pig anti-ProSAP2/Shank3 (1:500; marker #3; antibody kindly supplied by Dr. Tobias Böckers, University of Freiburg, Germany).
3. Incubate for at least 24 h at 4°C with a cocktail consisting of streptavidin conjugated to the fluorochrome Alexa Fluor™ 546 (1:200, marker #1), goat anti-guinea pig IgG conjugated to Alexa Fluor™ 488 (1:100), and goat anti-mouse IgG conjugated to Alexa Fluor™ 594 (1:200).
4. Rinse with Tris buffer (6.06 g/l aqua dest, pH 7.4). Mount in Tris buffer with gelatin (0.2 g/100 ml Tris buffer, pH 7.4).
5. Dry and coverslip with DPX (Fluka Chemie AG, Buchs, Switzerland). After coverslipping, slides are always stored in a freezer at −20°C. This cold storage is intended to reduce fading of the fluorochromes over time. Sections containing fluorescence prepared as long as 8 years ago in our laboratory and stored at −20°C still contain sufficient fluorescence to be of good use.
6. Shrinkage of the tissue can be a problem if conservation of the 3D shape is paramount. Since a section adheres to a solid glass surface, drying will cause shrinkage mostly in the *Z* direction and to a lesser degree in the *XY* direction. Deformation of shape will be inevitable. In addition to shrinkage in the *Z* direction comes the reduced resolution in the axial direction in the confocal instrument. Shrinkage by drying and mounting in DPX can reduce the thickness of a section 60–75% compared with its original "wet" thickness. A measure to reduce shrinkage and deformation is to mount and embed directly in Aquamount™ (Gurr; BDH, Poole, UK), or to apply measures discussed by Bacallao *et al.* (1995).

F. Troubleshooting

Insufficient penetration, crosstalk, and bleaching are the biggest problems encountered in multichannel confocal laser scanning. Insufficient penetration can be solved by several measures as listed in section "Introductory." Emission and excitation crosstalk can be excluded with some combinations of laser excitation wavelengths and fluorochromes (see section "Fluorochromes and Their Characteristics"). If excitation crosstalk cannot be avoided, then postacquisition dye separation can be attempted. Bleaching can be suppressed by the application of antifading agents to the preparations

and, at acquisition time, by being very conservative with the intensity setting of the lasers used for the excitation of the fluorochromes (see section "Controls"). Some fluorochromes resist bleaching much more than other fluorochromes. Remember that excessive bleaching in a *Z* series of images reveals itself as a one-way gradient over the frames of decreasing crispness, with structures becoming vague and finally merging with the background noise. The latter situation is devastating since surface-rendered 3D reconstruction is based on connecting voxels in the image series with corresponding gray levels. Thus, with bleached sections, 3D rendering is unreliable at least. Anticipating and preventing bleaching is therefore of vital importance. Several software solutions exist that recognize and allow correction for bleaching in *Z* series. The Huygens II software used by us is equipped with such an option.

Acknowledgments. The know-how discussed in this chapter has been collected in several years of intense collaboration with a number of persons. I am much indebted to Peter Goede, Luciënne Baks-te Bulte, and Mariska Vonck for their extremely skilful immunohistochemical assistance. Various confocal instruments were at our disposal by the kind collaboration of several institutions and persons: Jan van Minnen, Faculty of Biology, Vrije University (Zeiss LSM 410), Jeroen Beliën, Department of Pathology, VUMC (Leica TCS-SP), and Wolfgang Härtig and Jens Grosche, Paul-Flechsig Institute of Neuroscience, Leipzig, Germany (Zeiss LSM-510). The continuous care by Nico Blijleven for the hardware and software with which we did the deconvolutions and 3D reconstructions is much appreciated. Several graduate students contributed as well to improvements in scanning methodology: Helen Pothuizen, Bas Jasperse, Ivo van den Elskamp, Michel van den Oever, Cathrin Canto, Malika Dahmaza, Robert Schuit, and Johanna Ramirez-Reatiga. I especially thank Amber Boekel for looking very critically at the procedures.

REFERENCES

Bacallao, R., Kiai, K., and Jesaites, L., 1995, Guiding principles of specimen preparation for confocal fluorescence microscopy, In: Pawley, J. B. (ed.), *Handbook of Biological Confocal Microscopy*, New York: Plenum Press, pp. 311–325.

Bertero, M., Boccacci, P., Brakenhoff, G. J., Malfanti, F., and van der Voort, H. T. M., 1990, Three-dimensional image restoration and super-resolution in fluorescence confocal microscopy, *J. Microsc.* **157:**3–20.

Böckers, T. M., Bockmann, J., Kreutz, M. R., and Gundelfinger, E. D., 2002, ProSAP/Shank proteins—a family of higher order organizing molecules of the postsynaptic density with an emerging role in human neurological disease, *J. Neurochem.* **81:**903–910.

Böckers, T. M., Kreutz, M. R., Winter, C., Zuschratter, W., Smalla, K. H., Sanmarti-Vila, L., Wex, H., Langnaese, K., Bockmann, J., Garner, C. C., and Gundelfinger, E. D., 1999, Proline-rich synapse-associated protein-1/cortactin binding protein 1 (ProSAP1/CortBP1) is a PDZ-domain protein highly enriched in the postsynaptic density, *J. Neurosci.* **9:**6506–6518.

Brakenhoff, G. J., Blom, P., and Barends, P., 1979, Confocal scanning light microscopy with high aperture immersion lenses. *J. Microsc.* **117:**219–232.

Foster, M., and Sherrington, C. S., 1897, *A Text Book of Physiology, Part III: The Central Nervous System*, 7th ed., London: Macmillan.

Gerfen, C. R., and Sawchenko, P. E., 1984, A method for anterograde axonal tracing of chemically specified circuits in the central nervous system: combined *Phaseolus vulgaris*-leucoagglutinin (PHA-L) tract tracing and immunohistochemistry, *Brain Res.* **343:**144–150.

Gerfen, C. R., Sawchenko, P. E., and Carlsen, J., 1989, The PHA-L anterograde axonal tracing method, In: Heimer, L., and Zaborszky, L. (eds.), *Neuroanatomical Tract-Tracing Methods 2, Recent Progress*, New York: Plenum Press, pp. 19–48.

Gerlach, J., 1858, *Mikroskopische Studien aus den Gebiete der menschlichen Morphologie*, Erlangen, Germany: Enke.

Groenewegen, H. J., and Wouterlood, F. G., 1990, Light and electron microscopic tracing of neuronal connections with *Phaseolus vulgaris*-leucoagglutinin (PHA-L), and combinations with other neuroanatomical techniques, In: Björklund, A., Hökfelt, T., Wouterlood, F. G., and van den Pol, A. N. (eds.), *Analysis of Neuronal Microcircuits and Synaptic Interactions. Handbook of Chemical Neuroanatomy*, Vol. 8, Amsterdam: Elsevier Biomedical Press, pp. 47–124.

Hiesinger, P. R., Scholz, M., Meinertzhagen, I. A., Fischbach, K. -F., and Obermayer, K., 2001, Visualization fo synaptic markers in the optic neuropil of Drosophila using a new constrained deconvolution method, *J. Comp. Neurol.* **429:**277–288.

Holmes, T. J., Bhattacharyya, S., Cooper, J. A., Hanzel, D., Szarowski, D. H., and Turner, J. N., 1995, Light microscopic images reconstructed by maximum likelihood deconvolution, In: Pawley, J. B. (ed.), *Handbook of Biological Confocal Microscopy*, New York: Plenum Press, pp. 389–402.

Inoué, S., 1995, Foundations of confocal scanned imaging in light microscopy. In: Pawley, J. B. (ed.), *Handbook of Biological Confocal Microscopy*, New York: Plenum Press, pp. 1–14.

Jonkers, B., Sterk, J., and Wouterlood, F. G., 1984, Transcardial perfusion fixation of the CNS by means of a compressed-air driven device, *J. Neurosci. Methods* **12:**141–149.

Kano, H., van der Voort, H. T. M., Schrader, M., van Kempen, G. M. P., and Hell, S. W., 1996, Avalanche photodiode detection with object scanning and image restoration provides 2–4 fold resolution increase in two-photon fluorescence microscopy, *Bioimaging* **4:** 187–197.

Leranth, C., and Pickel, V. M., 1989, Electron microscopic preembedding double immunostaining methods, In: Heimer, L., and Zaborszky, L. (eds.), *Neuroanatomical Tract-Tracing Methods 2, Recent Progress*, New York: Plenum Press, pp. 129–172.

Longin, A., Souchier, C., Ffrench, M., and Bryon, P. A., 1993, Comparison of anti-fading agents used in fluorescence microscopy: image analysis and laser confocal microscopy study, *J. Histochem. Cytochem.* **41:**1833–1840.

Minsky, M., 1957, US patent no. 301467, Microscopy Apparatus.

Ono, M., Murakami, T., Kudo, A., Isshiki, M., Sawada, H., and Segawa, A., 2001, Quantitative comparison of anti-fading mounting media for confocal laser scanning microscopy, *J. Histochem. Cytochem.* **49:**305–311.

Palade, G. E., and Palay, S. L., 1954, Electron microscope observations of interneuronal and neuromuscular synapses, *Anat Rec.* **118:**335–336.

Palay, S. L., and Palade, G. E., 1955, The fine structure of neurons, *J. Biophys. Biochem. Cytol.* **1:**69–88.

Peters, A., Palay, S. L., and de Webster, F. H., 1991, *The Fine Structure of the Nervous System: Neurons and Their Supporting Cells*, 2nd ed, Oxford: Oxford University Press, 494 pp.

Platt, J. L., and Michael, A. F., 1983, Retardation of fading and enhancement of intensity of immunofluorescence by *p*-phenylendiamine, *J. Histochem. Cytochem.* **31:**840–842.

Rayleigh, L., and Strutt, J. W., 1891, On pin-hole photography, *Philos. Mag.* **11:**87–99.

Rosene, D. L., Roy, N. J., and Davis, B. J., 1986, A cryoprotection method that facilitates cutting frozen sections of whole monkey brains for histological and histochemical processing without freezing artifact, *J. Histochem. Cytochem.* **34:**1301–1315.

Sassoë-Pognetto, M., and Fritschy, J. -M., 2000, Gephyrin, a major postsynaptic protein of GABAergic synapses, *Eur. J. Neurosci.* **12:**2205–2210.

Shaw, P. J., 1995, Comparison of wide-field/deconvolution and confocal microscopy for 3D imaging, In: Pawley, J. B. (ed.), *Handbook of Biological Confocal Microscopy*, New York: Plenum Press, pp. 373–387.

Sheppard, C. J. R., and Choudhurry, A., 1977, Image formation in the scanning microscope, *Opt. Acta* **24:**1051–1073.

Snyder, D. L., Schulz, T. J., and O'Sullivan, J. A., 1992, Deblurring subject to nonnegativity constraints, *IEEE Trans. Sign. Proc.* **40:**1143–1150.

van der Voort, H. T. M., and Strasters, K. C., 1995, Restoration of confocal images for quantitative image analysis, *J. Microsc.* **158:**43–45.

Waldeyer, F., 1891, Über einige neuere Forschungen im Gebiete der Anatomie des Centralnervensystems, *Dtsch. Med. Wochenschr.* **17:**1213–1218, 1244–1246, 1267–1269, 1287–1289, 1331–1332, 1352–1356.

Webb, R. H., and Dorey, C. K., 1995, The pixilated image, In: Pawley, J. B. (ed.), *Handbook of Biological Confocal Microscopy*, New York: Plenum Press, pp. 55–67.

Wessendorf, M. W., 1990, Characterization and use of multi-color fluorescence microscopic techniques, In: Björklund, A., Hökfelt, T., Wouterlood, F. G., and van den Pol, A. N. (eds.), *Handbook of Chemical Neuroanatomy: Analysis of Neuronal Microcircuits and Synaptic Interactions*, Vol. 8. Amsterdam: Elsevier, pp. 1–46.

Wouterlood, F. G., Böckers, T., and Witter, M. P., 2003, Synaptic contacts between identified neurons visualized in the confocal laser scanning microscope. Neuroanatomical tracing combined with immunofluorescence detection of postsynaptic density proteins and target neuron-markers, *J. Neurosci. Methods* **128:**129–142.

Wouterlood, F. G., and Jorritsma-Byham, B., 1993, The anterograde tracer biotinylated dextran-amine: comparison with the tracer *Phaseolus vulgaris*-leucoagglutnin in preparations for electron microscopy, *J. Neurosci. Methods* **48:**75–88.

Wouterlood, F. G., Pattiselanno, A., Jorritsma-Byham, B., Arts M. P. M., and Meredith G. E., 1993, Connectional, immunocytochemical and ultrastructural characterization of neurons injected intracellularly in fixed brain tissue, In: Meredith, G. E., and Arbuthnott, G. W. (eds.), *Morphological Investigations of Single Neurons In Vitro. IBRO Handbook Series "Methods in the Neurosciences,"* No. 16, Chichester, UK: Wiley and Sons, pp. 47–74.

Wouterlood, F. G., van Denderen, J. C. M., Blijleven, N., van Minnen, J., and Härtig, W., 1998, Two-laser dual-immunofluorescence confocal laserscanning microscopy using Cy2- and Cy5-conjugated secondary antibodies: unequivocal detection of co-localization of neuronal markers, *Brain Res. Protoc.* **2:**149–159.

Wouterlood, F. G., van Haeften, T., Blijleven, N., Perez-Templado, P., and Perez-Templado, E., 2002, Double-label confocal laserscanning microscopy, image restoration and real-time 3D-reconstruction to study axons in the CNS and their contacts with target neurons, *Appl. Immunohistochem. Mol. Morphol.* **10:**85–102.

Wouterlood, F. G., van Haeften, T., Eijkhoudt, M., Baks-te-Bulte, L., Goede, P. H., and Witter, M. P., 2004, Input from the presubiculum to dendrites of layer-V neurons of the medial entorhinal cortex of the rat, *Brain Res.* **1013:**1–12.

Zaborszky, L., and Cullinan, W. E., 1989, Hypothalamic axons terminate on forebrain cholinergic neurons: an ultrastructural double-labeling study using PHA-L tracing and ChAT immunocytochemistry, *Brain Res.* **479:**177–184.

Zaborszky, L., and Heimer, L., 1989, Combination of tracer technqiues, especially HRP and PHA-L with transmitter identification for correlated light and electron microscopic studies, In: Heimer, L., and Zaborszky, L. (eds.), *Neuroanatomical Tract-Tracing Methods 2, Recent Progress*, New York: Plenum Press, pp. 49–96.